Challenge Journal of
STRUCTURAL MECHANICS

Vol.7 No.3 (2021)

Mindlin's theory buckling compressive strength dynamic analysis dynamic response earthquake finite element analysis finite element method mechanical properties operational modal analysis optimization pushover analysis railways reinforced concrete seismic analysis seismic design seismic isolation shallow foundations steel silo teaching-learning based optimization th[illegible]iate

TULPAR ACADEMIC PUBLISHING

ISSN 2149-8024

Challenge Journal of Structural Mechanics

E-mail: *cjsmec@challengejournal.com*

Web page: *cjsmec.challengejournal.com*

TULPAR Academic Publishing
www.tulparpublishing.com

Challenge Journal of Structural Mechanics

CONTENTS

Research Articles

TULPAR ACADEMIC PUBLISHING

Challenge Journal of Structural Mechanics

Research Article

A numerical study on influence of strain gradients on lattice rotation in micro-machining of a single crystal

Murat Demiral [a,*], Anish Roy [b], Vadim V. Silberschmidt [b]

[a] *Department of Mechanical Engineering, University of Turkish Aeronautical Association, 06790 Ankara, Turkey*
[b] *Wolfson School of Mechanical, Electrical and Manufacturing Engineering, Loughborough University, LE11 3TU, UK*

ABSTRACT

In latest years small scale machining has been widely used in advanced engineering applications such as medical and optical devices, micro- and nano-electro-mechanical systems. In micromachining of metals, a depth of cut becomes usually smaller than an average crystal size of a polycrystalline structure; thus, the cutting process zone can be localized fully indoors of a single grain. Due to the crystallographic anisotropy, development of small scale machining models accounting for crystal plasticity are essential for a precise calculation of material removal under such circumstances. For this purpose, a 3D finite-element model of micro-cutting of a single grain was developed. A crystal-plasticity theory accounting for gradients of strain, implemented in ABAQUS/Explicit via a user-defined material subroutine VUMAT, was used in the computations. The deformation-induced lattice rotations in micro-cutting of a single crystal were analyzed extensively.

ARTICLE INFO

Article history:
Received 9 May 2021
Revised 8 June 2021
Accepted 28 June 2021

Keywords:
Strain-gradient crystal plasticity
Orthogonal micromachining
Single crystal
Lattice rotation
Finite element analysis

1. Introduction

In latest years small scale machining has become popular in manufacturing of components with sizes of sub-millimeter or smaller used in advanced engineering applications such as medical and optical devices, micro- and nano-electro-mechanical systems. This process diverges significantly from conventional machining as uncut chip thickness is usually smaller than the crystal size of the sample; hence, instantaneous removal of the material takes place entirely within a crystal level. Since single crystals are strongly anisotropic in their mechanical behaviour, the cutting process naturally depends on crystallographic orientation as well as slip system and slip activity in single grain (Lee et al., 2000).

Deformation-induced lattice rotations, i.e. a texture-softening factor, reorientation or lattice spin, have attracted attention in the micromachining community, since a close connection is present between crystallographic shear, the leading mechanism ruling the deformation, and the resulting texture evolution (Zaafarani et al., 2006). A few researches characterized the observed phenomena using various techniques including non-destructive 3D electron backscattered diffraction (Lee et al., 2000), transmission electron microscopy (Lloyd et al., 2005) and 3D synchrotron diffraction method (Yang et al., 2004). Nahata et al. (2021) investigated the sub-surface microstructure in terms of the lattice rotation, recrystallization and shear bands after micromachining of aluminum single crystal experimentally. Lee and Zhou (1993) accounted for the texture softening factor in their analytical micro plasticity model to understand chip formation in micromachining.

Due to intrinsic inhomogeneity of deformation field in small scale machining tests, evaluating the obtained data is not simple. The computational methods are often used alternatively to understand its underlying mechanics. For instance, Zahedi et al. (2013) used a 3D combined finite element (FE)-smoothed particle hydrodynamics crystal plasticity model to study the influence of crystallography in machining of a copper single crystal. Similarly, Wang et al. (2020) developed a 2D crystal plasticity FE model to investigate the chip profile and shear angle, as well as their dependence on crystallography. Demiral

* *Corresponding author*. Tel.: +90-312-589-6112 ; E-mail address: mdemiral@thk.edu.tr (M. Demiral)
ISSN: 2149-8024 / DOI: https://doi.org/10.20528/cjsmec.2021.03.001

et al. (2014a) investigated the effect of grain orientation on the behavior of a single crystal using a FE model incorporating the strain-gradient and crystal plasticity in the constitutive equations. However, in none of the above studies, the texture evolution during micromachining of a single crystal was studied comprehensively.

In this study, a three dimensional finite-element study of micro-machining of a b.c.c. single crystal is performed. The role of strain gradients due to inhomogeneous plastic deformation in small scales on the response of the structure cannot be ignored; thus, they are considered in the constitutive equations. Their effects on the spin of the crystalline lattice and resulting deformation patterns are presented.

This paper is divided into five sections. Section 2 introduces the constitutive equations of the theory used in the simulations. Section 3 describes the details of the developed FE model. Section 4 shows the obtained results with their associated discussions. Section 5 presents the concluding remarks of the study.

2. Theory

In the simulations, an enhanced modelling scheme for a strain-gradient crystal-plasticity (EMSGCP) theory reported in Demiral et al. (2017) was used. In the following, a dot superposed on a symbol indicates a material time derivative and a bold symbol denotes a vector or a tensor. The constitutive equations are summarized as follows:

Elastic (F^e) and plastic (F^p) parts are the components of the deformation gradient F according to Eq. (1).

$$F = F^e F^p \tag{1}$$

The following flow equation rules the evolution of F^p

$$\dot{F}^p = L^p F^p \tag{2}$$

where L^p, the plastic velocity gradient, is expressed as

$$L^p = \sum_{\alpha=1}^{N} \dot{\gamma}^\alpha s^\alpha \otimes m^\alpha \tag{3}$$

In Eq. (3), $\dot{\gamma}^\alpha$ is the shearing rate on the slip system α. s^α and m^α are the slip direction and the slip-plane normal, respectively. A power-law representation is used for $\dot{\gamma}^\alpha$, as

$$\dot{\gamma}^\alpha = \dot{\gamma}_0^\alpha sgn\,(\tau^\alpha) \left|\frac{\tau^\alpha}{g_T^\alpha}\right|^n \tag{4}$$

Here $\dot{\gamma}_0^\alpha$ is the reference strain rate, τ^α is the resolved shear stress, n is the material constant related to its rate-sensitivity, g_T^α represents the strength of the slip system α at the instant time, and sgn($\boldsymbol{\Gamma}$) is the signum function of $\boldsymbol{\Gamma}$.

In this model, the *critical resolved shear stress* ($g_T^\alpha|_{t=0}$) is ruled by the initial strength of slip systems associated with statistically stored densities (SSDs) ($g_S^\alpha|_{t=0}$) and geometrically necessary dislocations (GNDs) ($g_G^\alpha|_{t=0}$). They are related to initial SSD ($\rho_S|_{t=0}$) and GND ($\rho_G|_{t=0}$) densities, respectively, via the constant, K:

$$g_T^\alpha|_{t=0} = \sqrt{(g_S^\alpha|_{t=0})^2 + (g_G^\alpha|_{t=0})^2} \tag{a}$$

$$g_S^\alpha|_{t=0} = K\sqrt{\rho_S|_{t=0}} \tag{b}$$

$$g_G^\alpha|_{t=0} = K\sqrt{\rho_G|_{t=0}} = K\sqrt{\rho|_{t=0}\left(\overline{S/V}\right)^2} \tag{c}$$

The GND density term considered the normalized surface-to-volume ($\overline{S/V}$) ratio of the component (Demiral et al., 2017). The slip strength during loading progresses due to SSDs (Δg_S^α) and GNDs (Δg_G^α) on the slip system as follows:

$$g_T^\alpha = g_T^\alpha|_{t=0} + \sqrt{(\Delta g_S^\alpha)^2 + (\Delta g_P^\alpha)^2} \tag{a}$$

$$\Delta g_S^\alpha = \sum_{\beta=1}^{N} h_{\alpha\beta}\Delta\gamma^\beta \tag{b}$$

$$\Delta g_G^\alpha = \alpha_T \mu\sqrt{b n_G^\alpha} \tag{c}$$

where $h_{\alpha\beta}$ is the slip-hardening modulus, α_T, μ, b and n_G^α represent the Taylor coefficient, the modulus of shear, the Burgers vector and the effective density of GNDs, respectively. The following hardening model was used to calculate $h_{\alpha\beta}$:

$$h_{\alpha\beta} = q h_{\alpha\alpha} (\alpha \neq \beta) \tag{a}$$

$$h_{\alpha\alpha} = h_0\, sech^2 \left|\frac{h_0\tilde{\gamma}}{g_T^\alpha|_{sat} - g_T^\alpha|_{t=0}}\right| \tag{b}$$

$$\tilde{\gamma} = \sum_\alpha \int_0^t |\dot{\gamma}^\alpha| dt \tag{c}$$

where h_0 denotes the initial hardening parameter, $\tilde{\gamma}$ is the cumulative shear strain on all slip systems, $g_T^\alpha|_{\text{sat}}$ is the saturation stress of the slip system α, q is the latent hardening ratio, considered to be 1. The effective GND density (n_G^α) equals to:

$$n_G^\alpha = \left|m^\alpha \times \sum_\beta s^{\alpha\beta} \nabla\gamma^\beta \times m^\beta\right| \tag{8}$$

Here $s^{\alpha\beta} = s^\alpha . s^\beta$ and $\nabla\gamma^\beta$ represents the gradient of shear strain for each slip system. In an enhanced model of crystal-plasticity (EMCP), Δg_G^α disappears as it does not consider the evolving GNDs. The models were implemented in the FE software ABAQUS/Explicit via the user-defined material subroutine (VUMAT) (Demiral et al., 2016).

In this study, the micro-machining of a single crystal β-brass having a b.c.c. crystalline structure is investigated. The active slip systems for this structure are {110}<111> (Ueda et al., 1980); thus, only this slip system set -among three potential system in b.c.c. materials- was activated in the computations. The respective planes and directions of the systems are presented in Table 1. Material constants and model parameters used in the simulations are given in Table 2.

Table 1. The planes and directions of slip systems for {110} <111> set

System	Plane	Direction
1	(0 1 1)	[1 -1 1]
2	(0 1 1)	[1 1 -1]
3	(1 0 1)	[-1 1 1]
4	(1 0 1)	[1 1 -1]
5	(1 1 0)	[-1 1 1]
6	(1 1 0)	[1 -1 1]
7	(0 -1 1)	[1 1 1]
8	(0 -1 1)	[-1 1 1]
9	(1 0 -1)	[1 1 1]
10	(1 0 -1)	[1 -1 1]
11	(-1 1 0)	[1 1 1]
12	(-1 1 0)	[1 1 -1]

Table 2. Material and model parameters used in simulations (Demiral et al., 2014a; Jona et al., 2001; Jia et al., 2012; Beyerlein et al., 2011).

Elastic properties			Density and damping parameters		
C_{11} (GPa)	C_{12} (GPa)	C_{44} (GPa)	ρ (kg m^{-3})	Linear bulk viscosity	Quadratic bulk viscosity
131.0	115.0	92.0	8500	0.06	1.2
Plastic properties					
$\dot{\gamma}_0^\alpha$ (s^{-1})	n	q	h_0 (MPa)	$g_T^\alpha\|_{sat}$ (MPa)	α_T
10^{-3}	20	1	294	60	0.8
K (MPa mm)	μ (GPa)	b (mm)	$\rho_S\|_{t=0}$ (mm^{-2})	$\rho\|_{t=0}$ (mm^{-2})	$\overline{S/V}$
0.04	27.12	2.56×10^{-7}	$6.8\ 10^5$	$5.0\ 10^4$	4.36

3. Finite Element Modelling of Micro-cutting

The FE modellings of structures have been widely used in the literature to investigate their responses when subjected to complex loading conditions (Ercan et al., 2015). Especially, the chip formation of a single crystal in micro-cutting process is multifaceted, where the crystal structure, crystal orientation and cutting direction play an important role in the formation of the chip. Its numerical model was developed. Details of the developed FE model simulating the orthogonal micro-cutting is shown in Fig. 1. The dimensions of the modelled part of a single-crystal workpiece were: length l = 20 µm, height h = 20 µm and width w = 0.48 µm. The sample was discretized using eight-node linear brick elements (C3D8) with a minimum element size of 60 nm in the process zone (resulted in 29600 elements). The rigid cutting tool was moving with a velocity of 1300 mm/s in the cutting direction (CD, [abc] in Fig. 1) (Demiral et al., 2014a). Its rake and clearance angles are both 0°. While, the depth of cut (a_p) equalled to 0.8 µm, the maximum cutting length was 1.20 µm. They were selected to ensure the formation of a chip. An element-deletion technique available in ABAQUS/Explicit (2013) was employed in our cutting simulations. A failure criterion based on the Taylor cumulative shear strain with a threshold value of 3.0 (represents the onset of damage) was used to delete the elements (Demiral et al., 2014a). Friction between the contacting bodies was ignored in the simulations (Demiral et al., 2014b).

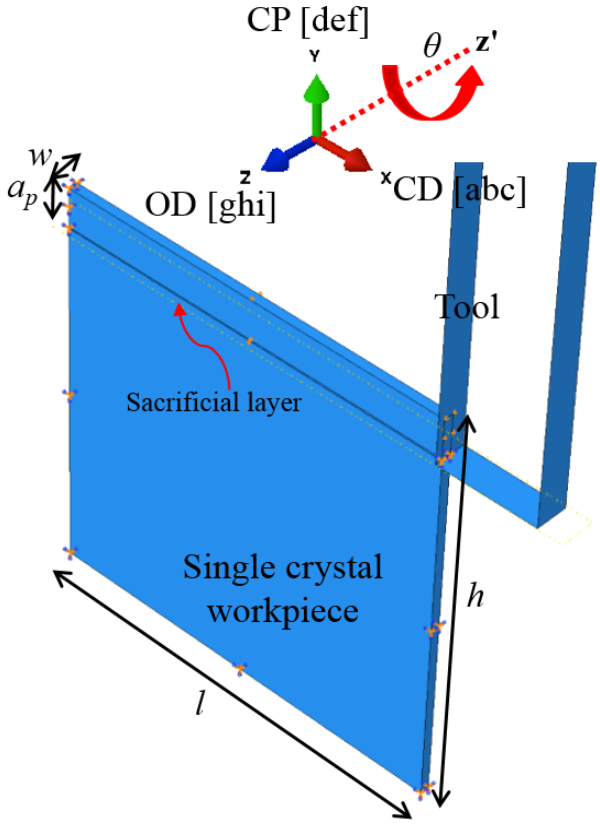

Fig. 1. Details of the developed FE model for micro-cutting of single-crystal β-brass.

4. Results and Discussion

In this section, the results from the numerical computations of micro-cutting of single-crystal β-brass are presented. To evaluate the influence of rotation angle θ for a grain with the [101] axis aligned with the observation direction (OD, [ghi] in Fig. 1) on the lattice rotations, three cutting directions, namely θ = 0°, 35° and 90°, were considered. The respective values are listed in Table 3.

Table 3. Orientations CD ([abc]) and CP ([def]) for various θ values for [1 0 1] axis aligned with the OD (see Fig. 1)

θ	0°	35°	90°
[abc]	[0 -1 0]	[-0.990 -2 0.990]	[-1 0 1]
[def]	[-1 0 1]	[-1 0.990 1]	[0 1 0]

Crystal reorientation in the workpiece material for the grain orientations analyzed is shown in Fig. 2. Here, lattice rotations about the OD-axis are compared. First, the lattice spin, i.e. induced lattice rotation, were distributed in the chip in a significantly different way for the cases investigated. It was observed that its magnitude was largest for θ = 90°, reaching some 65°, and smallest for θ = 0° with a maximum value of around 25°. It was found that while at θ = 35°, 90° the texture evolved in the chip in both positive and negative directions, at θ = 0° this occurred only in the negative direction. Dashed lines in Fig. 2 separate the regions with positive and negative lattice rotations in the deformed zone (representing the formation of a chip). In both orientations, for θ = 35°, 90°, crystal reorientation occurs in the opposite directions in the upper region of the chip and in the lower part. While the boundary between them is nearly vertical for θ = 35°, it is more horizontal for θ = 90°.

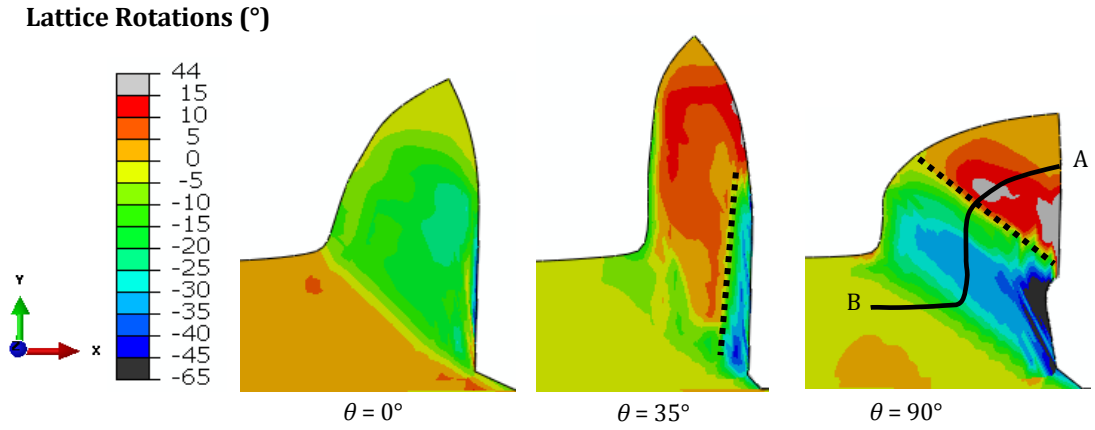

Fig. 2. Lattice rotation angles with their signs obtained by FE simulations of micro-machining at cutting length of 1.20 μm for various crystallographic orientations (Dashed line separates the regions in the chip with positive and negative lattice rotations).

There is a tight link between crystallographic shear, the key mechanism leading the deformation through slip systems, and the resulting grain reorientation. In connection with this, to understand the differences in the characteristics of the lattice rotations depending on the rotation angle θ, the role of activated slip systems was scrutinized. Fig. 3 presents a spatial 3D distribution of individual shear strain values on the active slip systems for θ = 90° of [1 0 1]. It was observed that slip systems 2, 5, 8, 9, 10 and 12 accommodated the overall shear in the workpiece, where the second/twelfth slip systems were the most active ones followed by the fifth/eighth systems and ninth/tenth systems in a row. The contributions of other slip systems were negligibly small; thus, they were not presented in Fig. 3.

The comparative individual contributions of various slip systems in the region of workpiece with higher shear activity ($\tilde{\gamma}$ larger than 0.05) for different θ values are presented in Fig. 4. It was noticed that, there existed only 4 active slip systems for θ = 0° with 5th and 8th systems carried around 62.6% of the overall shearing while the 2nd and 12th carried more than 30%. When θ was changed into 35°, significant changes were noted. The most dominant slip systems for θ = 0°, 5th and 8th, became less active with just 6.31% contribution for each, whereas the 9th and 10th systems took over their role involving in more than 50% of the total deformation. The activity of 2nd and 12th systems remained constant. Consequently, there were 6 slip systems ruling the deformation for θ = 35° as well as for θ = 90°, as explained above. Overall, the 9th and 10th systems did not participate in ruling the deformation for θ = 0°, whereas they were contributing significantly and non-negligibly for θ = 35° and 90°, respectively. These two slip systems seemed to be responsible for the sign change of the lattice rotations for the orientations with non-zero rotation angles observed above. Furthermore, the difference in terms of the active slip systems for different cutting directions affected chip morphology as observed in Fig. 2 (Demiral et al., 2014a; 2016).

The calculated magnitudes of shear angle for the cases investigated were 44°, 55° and 38° for θ = 0°, 35°, 90°, respectively (see Fig. 2). In ultra-precision machining, a continuous chip formation and good surface finish can be achieved for a chip having a larger shear angle (Lee, 1990). In connection with this, θ = 35° is preferable

among the cutting directions considered here in small scale cutting of brass single crystals for an enhanced surface finish.

FE simulations for $\theta = 90°$ were also performed using the EMCP theory. Compared to it, the EMSGCP theory exemplifies the involvement of strain gradients and their progress in an inhomogeneous cutting process. Lattice rotations along the path A-B in Fig. 2 is presented in Fig. 5 for the two theories. It was observed that the lattice spin had a larger variation on the chosen path when the EMCP theory was used. Since deformation-induced incompatibility in the lattice spin for a material point can be accommodated by GNDs in the EMSGCP theory, the distributions of lattice rotations are smoother when compared to that for the EMCP theory as expected for a physically reasonable strain-gradient theory (Niordson and Hutchinson, 2003; Demiral et al., 2014b).

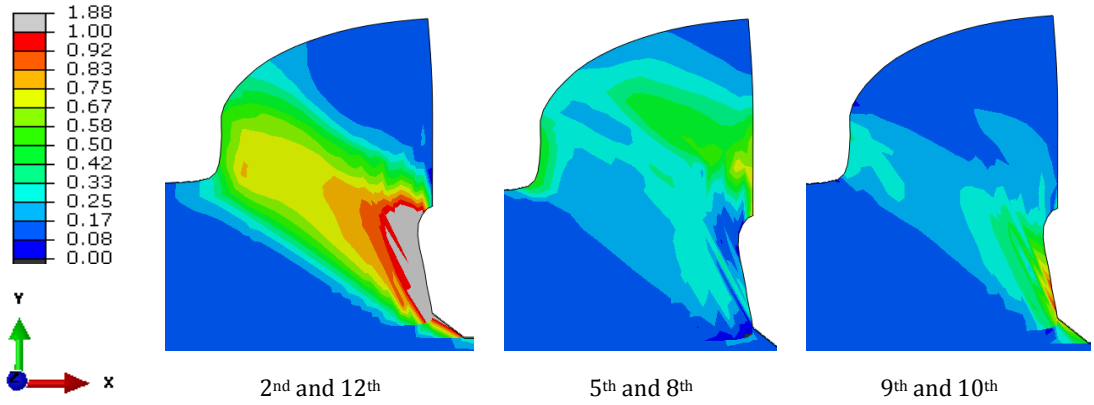

Fig. 3. Distributions of shear strains for different active slip systems on the single crystal workpiece at cutting length of 1.2 μm for $\theta = 90°$.

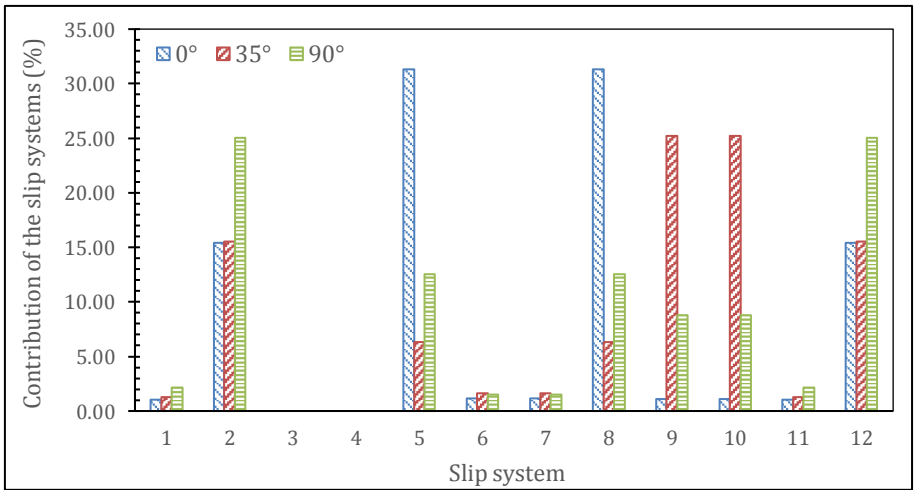

Fig. 4. Individual contributions of different slip systems (in %) on the workpiece material points with $\bar{\gamma}$ larger than 0.05 for different θ values.

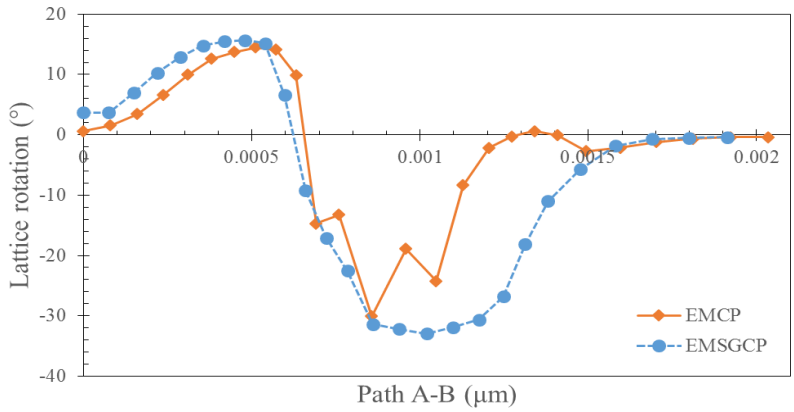

Fig. 5. Lattice rotation along path A–B in Fig. 2 at cutting length of 1.20 μm for $\theta = 90$ from numerical computations using different theories.

5. Conclusions

The properties of final products are dependent on the resultant texture. Understanding the establishment and progress of deformation texture can provide theoretical insight for texture control, thus enhancing properties of the material. In connection with this, in this paper, the reorientation of crystals in the brass single crystal in micro-machining for different grain orientations was scrutinized using an advanced model. Our study confirmed the following conclusions:

- The patterns of lattice spins varied significantly for the cutting directions investigated. While both positive and negative lattice rotations in the chip were observed for θ = 35°, 90°, they were only negative for θ = 0°.
- The contributions of different slip systems were observed to be different for different orientations of a single crystal. That affected the magnitudes and sign change in the lattice spin as well as the resulting chip morphology.
- A smoother distribution of lattice spins was obtained using the EMSGCP compared to the EMCP theory.

In the future, the model will be further developed to investigate the texture evolution in micro-machining of polycrystalline samples.

References

Beyerlein IJ, Mara NA, Bhattacharyya D, Alexander DJ, Necker CT (2011). Texture evolution via combined slip and deformation twinning in rolled silver–copper cast eutectic nanocomposite. *International Journal of Plasticity*, 27(1), 121-146.

Dassault Systemes (2013). Abaqus 6. 13 Analysis User Manual.

Demiral M, Roy A, El Sayed T, Silberschmidt VV (2014a). Influence of strain gradients on lattice rotation in nano-indentation experiments: A numerical study. *Materials Science and Engineering: A*, 608, 73-81.

Demiral M, Roy A, El Sayed T, Silberschmidt VV (2014b). Numerical modelling of micro-machining of fcc single crystal: influence of strain gradients. *Computational Materials Science*, 94, 273-278.

Demiral M, Roy A, Silberschmidt VV (2016). Strain-gradient crystal-plasticity modelling of micro-cutting of bcc single crystal. *Meccanica,* 51(2), 371-381.

Demiral M, Nowag K, Roy A, Ghisleni R, Michler J, Silberschmidt VV (2017). Enhanced gradient crystal-plasticity study of size effects in a β-titanium alloy. *Modelling and Simulation in Materials Science and Engineering*, 25(3), 035013.

Ercan E, Alver N, Nuhoğlu A (2015). Evaluation of material properties by NDT methods and FEM analysis of a stone masonry arch bridge. *Challenge Journal of Structural Mechanics*, 1(4), 168-172.

Jia N, Roters F, Eisenlohr P, Kords C, Raabe D (2012). Non-crystallographic shear banding in crystal plasticity FEM simulations: Example of texture evolution in α-brass. *Acta Materialia*, 60(3), 1099-1115.

Jona F, Marcus PM (2001). Structural and elastic properties of β-brass. *Journal of Physics: Condensed Matter*, 13(23), 5507.

Lee WB (1990). Prediction of microcutting force variation in ultra-precision machining. *Precision Engineering*, 12(1), 25-28.

Lee W, To S, Cheung C (2000). Effect of crystallographic orientation in diamond turning of copper single crystals. *Scripta Materialia*, 42(10), 937-945.

Lee WB, Zhou M (1993). A theoretical analysis of the effect of crystallographic orientation on chip formation in micromachining. *International Journal of Machine Tools and Manufacture*, 33(3), 439-447.

Lloyd SJ, Castellero A, Giuliani F, Long Y, McLaughlin KK, Molina-Aldareguia JM, Clegg WJ (2005). Observations of nanoindents via cross-sectional transmission electron microscopy: A survey of deformation mechanisms. *Proceedings of the Royal Society A: Mathematical, Physical and Engineering Sciences*, 461(2060), 2521-2543.

Nahata S, Moradi M, Picard YN, Kota N, Ozdoganlar OB (2021). Micromachining imposed subsurface plastic deformation in single-crystal aluminum. *Materials Characterization*, 171, 110747.

Niordson CF, Hutchinson JW (2003). On lower order strain gradient plasticity theories. *European Journal of Mechanics-A/Solids*, 22(6), 771-778.

Ueda K, Iwata K, Nakayama K (1980). Chip formation mechanism in single crystal cutting of β-brass. *CIRP Annals*, 29(1), 41-46.

Wang Z, Zhang J, Xu Z, Zhang J, Li G, Zhang H, Li Z, ul Hassan H, Fang F, Hartmaier A, Yan Y (2020). Crystal anisotropy-dependent shear angle variation in orthogonal cutting of single crystalline copper. *Precision Engineering*, 63, 41-48.

Yang W, Larson BC, Pharr GM, Ice GE, Budai JD, Tischler JZ, Liu W (2004). Deformation microstructure under microindents in single-crystal Cu using three-dimensional x-ray structural microscopy. *Journal of Materials Research*, 19(1), 66-72.

Zaafarani N, Raabe D, Singh RN, Roters F, Zaefferer S (2006). Three-dimensional investigation of the texture and microstructure below a nanoindent in a Cu single crystal using 3D EBSD and crystal plasticity finite element simulations. *Acta Materialia*, 54(7), 1863-1876.

Zahedi SA, Demiral M, Roy A, Silberschmidt VV (2013). FE/SPH modelling of orthogonal micro-machining of fcc single crystal. *Computational Materials Science*, 78, 104-109.

Challenge Journal of Structural Mechanics

Research Article

A comparative study on the structural performance of an RC building based on updated seismic design codes: case of Turkey

Ercan Işık [a,*]

[a] *Department of Civil Engineering, Bitlis Eren University, 13100 Bitlis, Turkey*

ABSTRACT

The destructive earthquakes and structural damages reveal the importance of the rules of earthquake-resistant structural design. The need of update and renewal of these rules periodically become inevitable as a result of scientific developments, innovations in construction technologies and building materials. Turkey which is an extremely region in terms of seismicity was adapted to these changes through time. The last five seismic design codes (1968, 1975, 1998, 2007 and 2018) were taken into account within the scope of this study. The differences in dimension and material grades of structural elements such as columns as beams have been compared in detail for each code. Three different analysis types have been performed for a 4-story reinforced-concrete model such as eigenvalue, pushover and dynamic time-history via the minimum conditions for these elements in each code. The natural vibration period of the building was obtained with empirical formulas stipulated in different codes for the sample RC building, additionally. The size and the type of the materials used in beams and columns within the last five codes have been changed. We see that the changes in these two important parameters which affect the behavior of buildings during an earthquake, enhance the performance of the building. It has been revealed that changes and renewals in seismic design codes are a necessity and gain. It has been clearly revealed that each amended code increases the stiffness and enhance the seismic capacity of a structure. Each updated seismic design code is aimed to complete the deficiency of the previous one. The results revealed that there are changes to be made to increase the seismic capacity of the structure at the point of reducing earthquake damage.

ARTICLE INFO

Article history:
Received 18 March 2021
Revised 8 June 2021
Accepted 7 July 2021

Keywords:
Turkey
Reinforced concrete
Codes
Pushover
Time-history
Eigenvalue

1. Introduction

The large scale of earthquake damages reveals the importance of the rules of earthquake-resistant structural design. This situation is not so different in Turkey, as all over the countries which are characterized by highest levels of seismic risk. Recent earthquakes that occurred in Turkey are the 2011 Van Earthquake (Mw=7.2), the 2020 Sivrice (Elazığ) Earthquake (Mw=6.7) and the 2020 İzmir Earthquake (Mw=6.9). The structural damages caused by these earthquakes have shown the importance of these rules. These rules and their applicability in practice emerge as an important point for the loss of life and property in the regions where earthquakes are ineluctable. The development in construction technologies and building materials, modern approaches and the use of software in structural analysis led to some compulsory changes and renewals in the codes to meet the needs of the construction industry. Besides these, the data obtained from earthquake damages have important contributions into the progress of seismic design code. Turkey has been made important amendments to these rules as a result of the tragic earthquakes. Some of these rules have been updated or completely amended or new additions were made on different dates. It finally came into force on January 1, 2019, and took its final version.

* *Corresponding author*. Tel.: +90-434-228-0030 ; Fax: +90-434-222-9145 ; E-mail address: eisik@beu.edu.tr (E. Işık)
ISSN: 2149-8024 / DOI: https://doi.org/10.20528/cjsmec.2021.03.002

The amendments in reinforced-concrete (RC) structural elements and systems can be observed easily within every new code.

The first rules regarding earthquakes in Turkey were issued in the period of II Bayezid, after the earthquake which caused approximately 13.000 deaths in Istanbul in 1509 (Kemaloğlu, 2015). The first regulation was prepared after the 1939 Erzincan earthquake, which caused about 33.000 deaths in 1939 (Öztürk, 2018). This was published in 1940 as "Italian Building Instructions for Construction in an Earthquake Zone" (Alyamaç and Erdoğan, 2005). After this date, due to developments in engineering technologies the codes have been constantly updated by taking into account the structural features that cause significant losses in earthquakes (Işık et al., 2021). Ten different seismic design codes have been used in Turkey up to now which came into force in 1940, 1944, 1949, 1953, 1962, 1968, 1975, 1998, 2007 and 2018. The first four regulations contain only earthquake-related rules. The 1962–1998 regulations include rules on all types of disasters such as floods, fires and earthquakes. The earthquake related rules were prepared separately with the 2007 code. The loss of life and property (Mw=7.2 and Mw=5.6) encountered in 2011 Van earthquakes revealed the need for updating the latest code. Each regulation was made to eliminate the specified weaknesses in the previous regulation. Especially with the last two regulations, very significant changes have been made. The current regulation has been prepared in much more detail. The structural system element dimensions and the material grades, which have significant effects on earthquake behavior of structures, were also modified by these changes.

The changes in the minimum requirements which are suggested for the structural system elements are very important. These values become more important especially for RC buildings that suffer more damage in earthquakes. The majority of the existing structures and the structures to be built and already exists in Turkey consist of RC structures. Therefore, the legal regulations to be made regarding RC structures have a greater importance. Poor/low strength of materials and dimension take an important place among the causes of earthquake-led damages in such structures. Lack of material strength and dimensions increases the amount of damage, especially in RC structures that do not receive engineering services. When these two parameters are poor, the structural strength mechanism weakens and it can be damaged even at values below the foreseeable loads in RC structural elements. Damages are generally associated with the low strength of concrete in RC buildings. The mechanical properties of concrete have an important place in terms of safety in RC structures. The grade of reinforcement is also one of the parameters which directly affects the structural strength of the structure. When the concrete dimensions do not meet the standard requirements the level of potential damage also increases. There are numerous publications on examining the changes in the codes in Turkey. These publications generally compared the last two earthquake regulations. Base shear forces, displacements, periods, target displacements and spectral acceleration curves have been compared within these studies (Işık et al., 2020a, 2020b; Aksoylu et al., 2020; Aksoylu et al., 2019a; Keskin and Bozdoğan, 2018; Koçer et al., 2018; Karaşin et al., 2020; Bozer, 2020; Karaca et al., 2020). In this study, not only the last two but the last five earthquake codes are taken into account.

The last five seismic design codes in Turkey are taken into account within the scope of this study. The study has been limited by considering the minimum material grade and dimensions for column-beam elements which take place in 1968, 1975, 1998, 2007 and 2018 codes. This study aims to examine the change of these parameters in the codes of different dates and to reveal to what level the building performance is affected. Eigenvalue, pushover and dynamic time-history analyses are performed for a 4-story RC sample building via the minimum dimension and material grades for each code. Furthermore, empirical formulas are used to compare these five codes with respect to natural vibration periods of the building under consideration. The period, base shear force, elastic/effective stiffness, target displacement and total support force/moment are obtained through the analysis of the sample RC building. In the first part of the study, some information is given about the codes under consideration. After the explanations on the modelling of sample RC building, the process of the formation and the damping of the natural vibration period of the building are analyzed. Subsequently, information about the structural analysis used in this study such as eigenvalue, pushover and dynamic time-history is given. The results are shown with the help of tables and figures. Finally, the results are compared and some conclusions are derived from the analysis. This study will be one of the first studies to be carried out considering both the last five seismic design codes and the minimum dimension and material grade.

2. Advance in Seismic Design Codes in Turkey

Earthquakes are critical to experiment with the structures under horizontal loads. The data obtained on earthquake damages are very important in understanding the earthquake behavior of buildings. These damages must be obtained and interpreted correctly in terms of revealing the deficiencies in the construction and design rules (Işık, 2016, 2018; Hadzima-Nyarko and Sipos, 2017; İnel and Meral, 2016; Yakut, 2004; Xian et al., 2016). This earthquake-damaged data can be used for different purposes. One of the main purpose of the gathered data is that it can be used to revise or to completely renew the standards and the codes related to the building. It also helps to identify the deficiencies in the code. In parallel with the development of technology, new standards and codes have been imposed in the construction process to minimize the earthquake-led losses.

The first regulation about disasters based on edict issued by II. Bayezid after the earthquake that caused approximately 13.000 deaths in Istanbul on 14.09.1509 (Kemaloğlu, 2015). However, the first regulation was prepared after the 26 December 1939 earthquake that occurred in Erzincan which had

caused substantial destruction (Öztürk, 2018). The first code has been published in 1940 as "Italian Building Instruction for Construction in Earthquake Region" (Alyamaç and Erdoğan, 2005). This code has been continuously updated, by taking into account the developments in engineering technologies and significant losses in earthquakes. Ten seismic design codes were entered into force, in the years 1940, 1944, 1949, 1953, 1962, 1968, 1975, 1998, 2007 and 2018. The codes that have been published up to now are shown in Table 1.

Table 1. Historical change of seismic design codes in Turkey.

Year	Code Name
1940	Italian Building Instruction for Construction in Earthquake Region
1944	Temporary Construction Instruction in Earthquake Region
1949	Turkey Ground Shakes Regions Building Code
1953	Code on Structures to be Made in Disaster Areas
1962	Code on Structures to be Made in Disaster Areas
1968	Code on Structures to be Made in Disaster Areas
1975	Code on Structures to be Made in Disaster Areas
1998	Code on Structures to be Made in Disaster Areas
2007	Code on Buildings to be Built in Earthquake Zones
2018	Turkish Building Earthquake Code

The rules of earthquake-resistant structural design were included in the disaster regulations at first, in Turkey. As these codes were into force, earthquakes continued to happen over time so that it has been realized that the codes are insufficient and the need has become clear for governments to update or to renew the regulations. With the gained experience and developing technology, current regulations were tried to be progressed and updated. The major subject in these promulgated codes has always been earthquakes; hence these codes are also referred to as earthquake codes (Alyamaç and Erdoğan, 2005). The last five seismic design codes considered in this study is given in Table 2.

Table 2. The codes that used in this study.

Year	Code	Abbreviation (in Turkish)
1968	Specification for Structures to be Built in Disaster Areas	ABYYHY-1968
1975	Specification for Structures to be Built in Disaster Areas	ABYYHY-1975
1998	Specification for Structures to be Built in Disaster Areas	ABYYHY-1998
2007	Turkish Earthquake Code	DBYBHY-2007
2018	Turkey Building Earthquake Code	TBDY-2018

The progress of code is directly related with the development and elaboration of structural analysis and calculations, experiences gained due to earthquake-led structural damages and emerging engineering technology. Taking into account all of these, the result is that change is inevitable. Every new code is an achievement in terms of the rules of the earthquake-resistant structural design. Therefore, an important step has been taken in terms of modern disaster management thanks to the minimization of possible damage levels.

2.1. 1968 Code (ABYYHY-1968)

Some suggestions have been made regarding protection from floods and fire disasters other than earthquakes with this code. The general characteristics of RC building elements are mentioned, and the rules regarding dimension and reinforcement are included, with the increasing importance of RC buildings during this period. Moreover, information is visualised by drawings in these regulations hence it is better understood. The most important difference of this code from the previous ones is that, it mentions the rules of RC structural elements and the earthquake analysis becomes more detailed (Alyamaç and Erdoğan, 2005; ABYYHY-1968). The 1968 code generally includes ways of protection and the rules of design for different types of natural disasters. The RC term was used for the first time in this regulation. The RC structures had been recommended to be constructed quite simply in a rectangular or square shape without any overhangs. Criteria on materials and dimensions related to structures to be built as RC was given for different

ground conditions. Considering the solidity of the ground type, three different ground type have been accepted in this code. However, ground type classification has not been made according to any parameter such as shear wave velocity, SPT, etc.

2.2. 1975 Code (ABYYHY-1975)

The country is divided into four different earthquake zones with this code. A large part of the building stock consists of RC buildings in this period. It is a successful work according to the time in the code. The dimensions and reinforcement values given for RC elements are at a sufficient level in earthquakes. Earthquake forces calculations are made in detail according to many parameters with this code. Many deficiencies that caused heavy damage in earthquakes were observed and corrected in this code. The subject of repair and RC wall has been given in wide coverage and related rules are explained. The effect of local soil conditions has been taken into consideration in more detail in earthquake analysis in this code. The acceleration spectrum coefficients were determined and it was requested to be taken into account when finding earthquake forces (Alyamaç and Erdoğan, 2005; ABYYHY-1975). The 1975 code has been published under the titles of protection from the disasters of floods, fire and earthquake, and the details were stated in subheadings. Building importance level and live load reduction factors were first stated in this code. It has been made compulsory to use vibrators and concrete mixers in concrete casting. This is an updated version of the 1968 code. RC structural elements and limit values related to sectional dimensions were included also in this code. Four different ground types were determined by considering the shear wave velocity. The ground type effect is taken into account as a function of the ground dominance period. Elastic design spectrum is used for the first time in this regulation.

2.3. 1998 Code (ABYYHY-1998)

This code was made complete for a significant amount of earthquake resistant building design. It has a very safe design approach in this code, even considering the standards and regulations in other developed countries. Horizontal and vertical irregularities in the buildings have started to be taken into consideration with this code (Alyamaç and Erdoğan, 2005; ABYYHY-1968). This code, which was prepared in 1997 and entered into force in 1998, had been published under the titles of protection from the disasters of floods, fire and earthquake, and the details were stated in sub-headings, as the 1975 code. This code comprises some rules related to material properties and sectional dimensions in buildings similar to the other disaster codes. The ground types are classified in four different ways, similar to the 1975 code. Ground type classification was made by considering shear wave velocity, standard penetration, relative stiffness and free pressure strength. Soil liquefaction is also specified with this code.

2.4. 2007 Code (DBYBHY-2007)

The need to update the 1998 code has arisen after the major losses arising from İzmit (Gölcük) earthquake with Mw=7.6 magnitude and Düzce earthquake with Mw=7.2 magnitude in 1999. The preparation of this code was started in 2004 and it came into force in 2007. The biggest difference of this code from the previous codes, as can be understood from the name of the code, is that it includes only the rules about buildings to be built in earthquake zones. It contains earthquake-resistant rules for masonry, steel and RC structures. A different section has been added, which includes the foundation and the design rules of the foundations. The evaluation and strengthening of existing structures were mentioned for the first time with this code. This code has been regulated as more detailed and progressed from previous codes. It has been made mandatory to use ready-mixed concrete in RC buildings. Additionally, ground types are classified in four different ways, similar to the 1998 code.

2.5. 2018 Code (TBDY-2018)

Considering the major losses arising from the earthquakes that occurred after 2007, Van earthquake (2011) with Mw=7.2 magnitude and Van (Edremit-2011) earthquake with Mw=5.6 magnitude, in particular, this earthquake code has been revealed in 2018 and came into effect on January 1, 2019. This code contains a lot of details compared to previous codes. The most notable amendment in this code is the usage of site-specific design spectra. The Turkish Earthquake Hazard Map has been started to be used in the recently updated code instead of defined seismic zones. The site-specific seismic hazard evaluation is the main advantage of the new seismic code. The earthquake parameters obtained from regions differentiated via large-scale zoning by the previous code are selected locally through the new code. It is worth mentioning to this update yields more reasonable evaluations in structural performance. In addition, while only the horizontal elastic design spectrum was being used in the previous code, both horizontal and vertical elastic design spectra were started to be used with this code. Rules related to wooden and mixed-functional structures are also included in this code. Six different ground types were accepted by combining different ground types and groups in the previous regulation. As a result, the norms of earthquake-resistant structural design, which was introduced in 1940 for the first time in Turkey, have been continuously updated, taking into account the developments in engineering technologies and losses in earthquakes. Each new earthquake code appears in more detail, comprehensively and scientifically than the previous code.

3. The Properties of Sample RC Building

The last five codes were promulgated on different dates were considered within the scope of this study. The minimum concrete grade, reinforcement grade, col-

umn and beam dimensions, number and range of reinforcement were selected as variables. The minimum conditions are taken into account for each variable to be able to compare in structural analysis. The amendments of these parameters in the last five codes were examined. The changing of these parameters in the different codes were given in Table 3.

The minimum cross sections of the columns and beams according to the codes were given in Fig. 1 and Fig. 2, respectively.

Table 3. The changing of the structural properties considered in this study.

Parameter	1968	1975	1998	2007	2018
Concrete Grade	C12	C14	C16	C20	C25
Reinforcement Grade	S220	S220	S220	S420	S420
Columns Dimensions (mm)	250*250	250*250	250*300	250*300	300*300
Beams Dimensions (mm)	150*300	200*300	250*300	250*300	250*400
Beam Lower Reinforcement	2ϕ12	2ϕ12	3ϕ12	3ϕ12	3ϕ12
Beam Upper Reinforcement	2ϕ12	2ϕ12	2ϕ12	2ϕ12	2ϕ12
Longitudinal Reinforcement	4ϕ14	4ϕ14	4ϕ16	4ϕ16	6ϕ14
Transversal reinforcement (mm)	ϕ6	ϕ8	ϕ8	ϕ8	ϕ8
Spacing of Transversal reinforcement (mm)	250	200	200	200	200

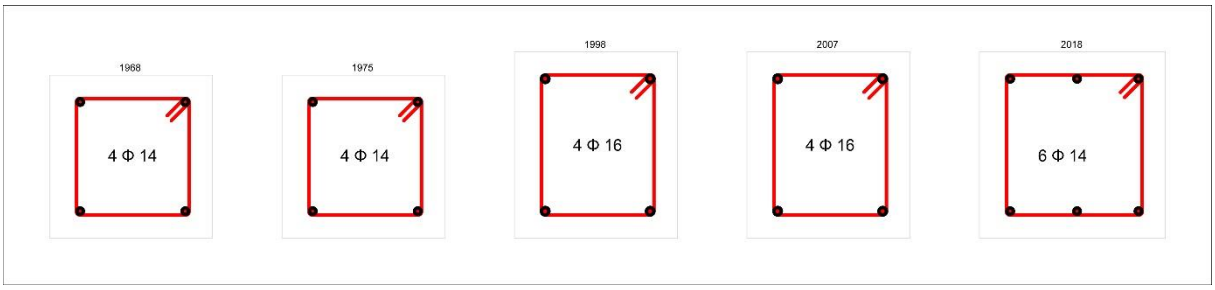

Fig. 1. Minimum cross-sections of columns.

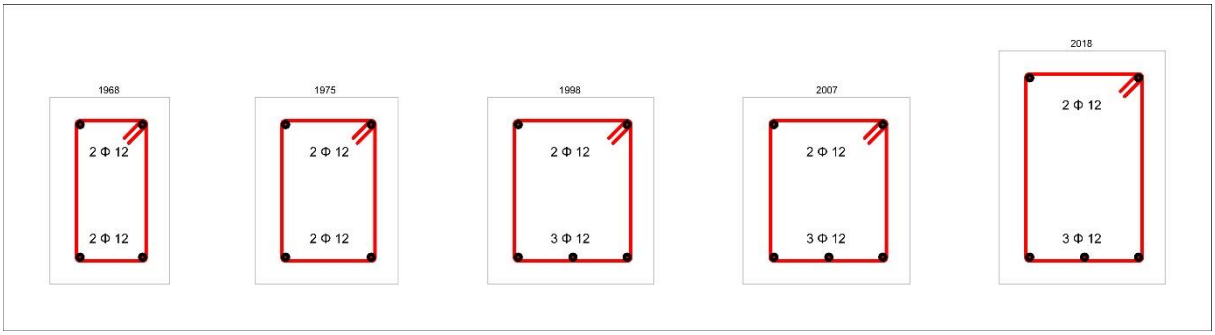

Fig. 2. Minimum cross-sections of beams.

Analyses were performed on academically licensed Seismostruct software (Seismosoft, 2018). Dead and incremental loads were applied to each building model and these values remained constant in all building models. Incremental load value was considered as 5kN and dead load value was 5kN/m. The wizard feature in the software was used while modeling the building. The wizard feature automatically activates the calculation of the target displacement in the case of pushover analysis. Target displacement was determined as 0.24 m by the wizard feature, which is constant in all building models. A sample RC structure with a total size of 20*20m has been selected as to be four spacing, 5 m each, in both X and Y directions. The blueprint of the sample RC building was given in Fig. 3.

The same blueprint was taken into consideration for each code. The minimum conditions obtained for the parameters considered within the scope of this study were selected as variables. In all the building models, local soil type, building importance level and damping ratio were indicated with the same values. The two-dimensional model obtained for the sample RC structure is used in this study and the applied loads are given in Fig. 4. The three-dimensional model obtained for the sample RC structure used in this study, and applied loads were given Fig. 5.

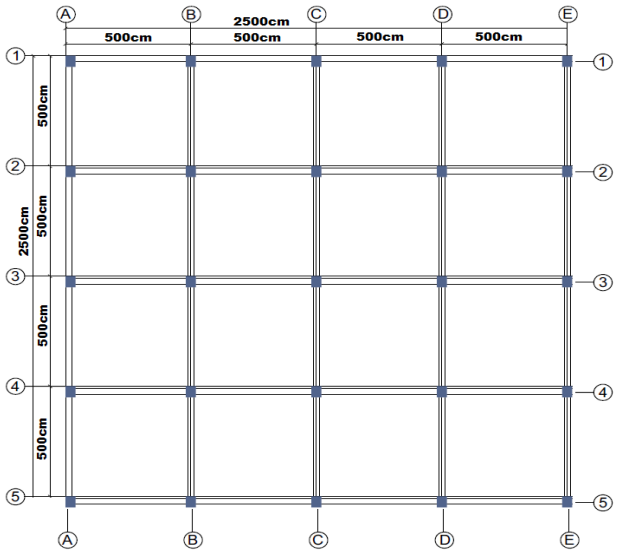

Fig. 3. The blueprint of sample RC building.

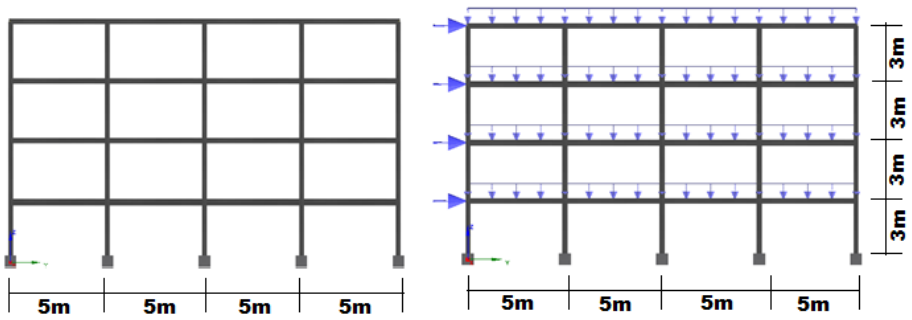

Fig. 4. 2D model and applied loads.

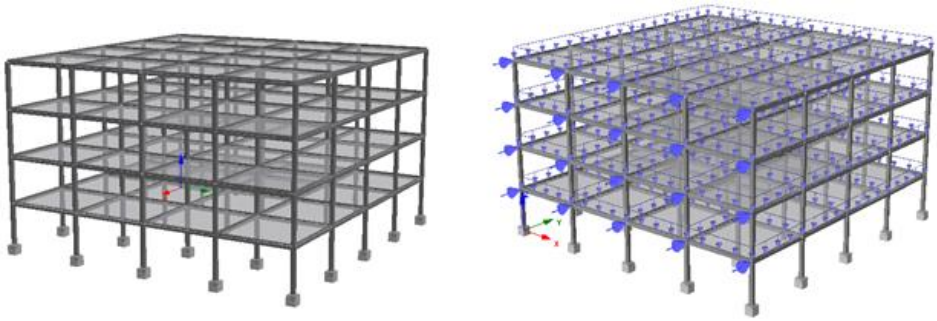

Fig. 5. 3D model and applied loads.

It is a fact that the behaviour of building materials under load can be determined using some mathematical models, which is vital in building design and evaluation. The nonlinear concrete model (Mander et al.,1998) and steel model (Menegotto and Pinto, 1973) were used for concrete and steel material. The stress-strain relationship of the material models considered for these models is demonstrated in Fig. 6.

4. Comparison of Natural Vibration Period

The natural vibration period of the structures is one of the important dynamic properties of the building. The period depends on the weight of the structure and the rigidity of the structural system against horizontal loads. Although natural vibration periods of structures can be calculated by analytical methods, first mode vibration periods can be calculated with empirical formulas in seismic design code in many countries (Aksoylu et al., 2020; Jamadin et al., 2020; Aksoylu ve Arslan, 2019b; Kutanis et al., 2017). The comparison of the natural vibration periods was made depending on the empirical formulas between the seismic design codes under consideration.

In the 1968 code, unless the calculation is made according to experimental or reliable technical data, the building fundamental period of vibration will be calculated as follows.

$$T = (0.09 \cdot H)/\sqrt{D} \quad (1)$$

where, H is the height of the building from the foundation base and D is the width of the building parallel to the direction of the lateral force affecting the building.

In the 1975 seismic design code, the building natural vibration period can be calculated, as specified in the 1968 code. Also, in this code, the period can be calculated empirically with;

$$T = (0.07 - 0.10) \cdot N \quad (2)$$

where, N indicates the total number of floors above the building foundation level. The coefficient will be chosen according to the rigidity of the structure. The coefficient of 0.10 will be used in structures consisting of only RC frames.

The empirical formula of the natural vibration period changed and became the following with the 1998 code;

$$T_1 = C_t \cdot H_N^{3/4} \quad (3)$$

No empirical formula was suggested in the 2007 code. However, in buildings with floor numbers N>13, excluding the basement floor (s), the natural period will not be taken higher than 0.1N.

In TBDY-2018, it is stated that two formulas can be used in the calculation of the natural vibration period of the building, regardless of the building type, the presence of infill wall, local ground type and many other parameters. The first one is the Rayleigh formula, which can be used at any time and under any condition. The other one is the empirical formula which is recommended if certain conditions are met. Empirically recommended formula is;

$$T_{PA} = C_t \cdot H_N^{3/4} \quad (4)$$

The sample building model under consideration is RC framed and consists of 4-story and 12 meters high. The comparison of the natural vibration periods which are empirically obtained for the sample building was given in Table 4.

Table 4. Comparison of the empirical natural vibration periods.

Code	Empirical Formula	Natural period (s)
1968	$T = (0.09 \cdot H)/\sqrt{D}$	0.241
1975	$T = (0.09 \cdot H)/\sqrt{D}$	0.241
1975	$T = (0.07 - 0.10) \cdot N$	0.400
1998	$T_1 = C_t \cdot H_N^{3/4}$	0.451
2007	There is no empirical formula.	
2018	$T_{PA} = C_t \cdot H_N^{3/4}$	0.644

5. Analysis Results

The first type of analysis considered in the study was eigenvalue analysis. All structure is subjected to vibrational movement under the effect of an earthquake. These movements are a combination of harmonic modes. Mode shapes and natural frequency for any structure can be obtained by eigenvalue analysis. Structure-related modal period, frequency, modal participation factors, effective modal masses and their percentage values can be achieved by eigenvalue analysis (Luo et al., 2017; Antoniou and Pinho, 2003; Seismossoft, 2018; Kutanis et al., 2017; Nikoo et al., 2017; Zuo and Zha, 2018). In this study, in order to determine the earthquake performance of building models pushover analysis has been used. This analysis examines the structure's behaviours under earthquake loads in a nonlinear situation. Through this analysis, it's possible to have enough information or data about the seismic demands of structural systems and components stemmed from the motion of the ground. This analysis can be implemented in both directions. It is easy to show the behaviour of a building in the inelastic region. The base shear force and peak displacement obtained from this analysis provide the capacity curve of the building. To obtain this curve, the lateral forces are increased monolithically until the displacement of the top of the building reaches a predetermined displacement value. The pushover curve is a diagram obtained by geometrically combining the intersection points on an interaction diagram of the roof displacement values corresponding to the base shear forces under the applied load by increasing the structure from zero to unstable (Fajfar, 1999; Chopra and Goel, 2002; Antoniou and Pinho, 2003; Eslami and Ronagh, 2014; Işık and Kutanis, 2015; Hadzima-Nyarko et al., 2016; Estêvão and Oliveira, 2015). Typical pushover and idealized capacity curve was given in Fig. 7.

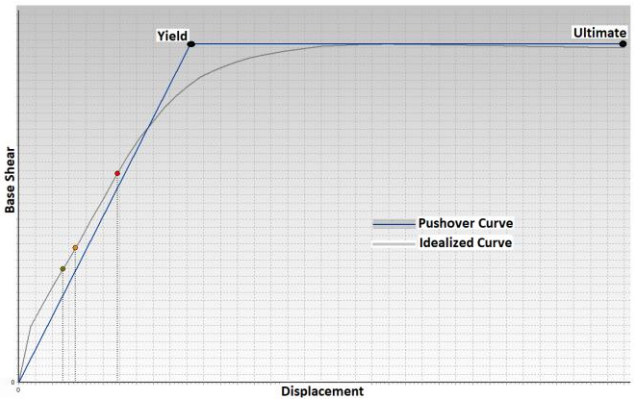

Fig. 7. Typical pushover and idealized capacity curves.

Besides, estimation of the linear and inelastic behaviour of a building exposed to earthquake loads is a commonly used dynamic time-history analysis tool. The direct integration of the equation of motion can be taken by using the numerical damped α integral algorithm or the Newmark-beta method. The automatic time-step ad-

justment ensures obtaining optimum accuracy and efficiency. Modelling of seismic effects is provided by defining acceleration load curves to the structural loadings. Different curves can be defined in each structural loading, thus, the representation of asynchronous ground motions is allowed (Antoniou and Pinho, 2003). El Centro Site Imperial Valley Irrigation District seismogram was taken into consideration within the scope of this study (Vibrationdata.com, 2020). Figure 8 shows the acceleration - time graph of this earthquake.

The displacement values were obtained for three different points on the idealized curve. The first value refers to the displacement (d_y) at the moment of yield, the second value refers to intermediate (d_{int}) and the third value refers to target displacement. The effective stiffness of cracked sections is obtained by using the prescribed stiffness reduction coefficients of the elastic stiffness value (Çağlar et al., 2015; Ugalde et al., 2020; Wilding and Beyer, 2018). The values of elastic stiffness (K_{elas}) and effective stiffness (K_{eff}) were calculated separately for all buildings model. In the structural analysis, the limit states are given in Eurocode-8, Part 3 (Eurocode 8, 2005; Pinto and Franchin, 2011) were taken into consideration for damage estimation that used worldwide. The limit states for damage estimation are presented in Table 5, according to Eurocode-8. These values were calculated separately for all codes.

Table 6 shows the results obtained in the X-direction for eigenvalue and pushover analysis for the sample RC building, while Table 7 shows in the Y-direction. The total support forces and total support moments are calculated based on load factors for each building model and results were given in Table 8.

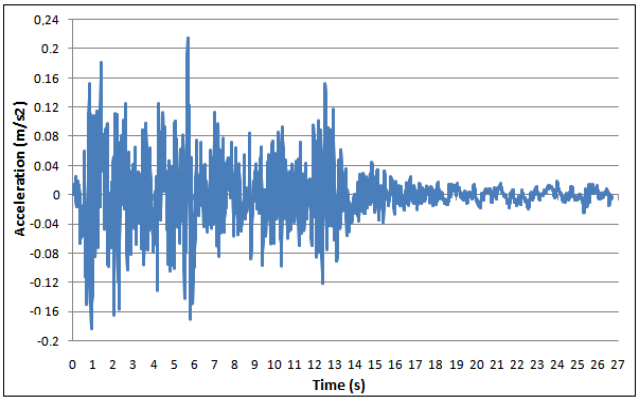

Fig. 8. The acceleration - time graph for El Centro earthquake.

Table 5. Limit states in Eurocode 8 (Part 3) (Eurocode, 2005; Pinto and Franchin, 2011).

Limit State	Description	Return period (year)	Probability of exceedance in 50 years
Limit state of damage limitation (DL)	Only lightly damaged, damage to non-structural components economically repairable	225	0.20
Limit state of significant damage (SD)	Significantly damaged, some residual strength and stiffness, non-structural components damaged, uneconomic to repair	475	0.10
Limit state of near collapse (NC)	Heavily damaged, very low residual strength & stiffness, large permanent drift but still standing	2475	0.02

Table 6. The comparison of analysis results in X direction.

Code	Period (s)	Base shear (kN)	Displacement (m)	K_{elas} (kN/m)	K_{eff} (kN/m)	DL (m)	SD (m)	NC (m)
			0.0728					
1968	0.569467	414.16	0.1009	10951.29	5675.08	0.0455661	0.0584537	0.1013381
			0.240					
			0.0633					
1975	0.550027	496.9	0.1008	15774.23	7851.34	0.0392367	0.0503342	0.0872617
			0.240					
			0.0653					
1998	0.545897	733.06	0.096	24367.73	11224.86	0.0403558	0.0517698	0.0897506
			0.240					
			0.0889					
2007	0.530264	901.59	0.1536	25863.25	10144.54	0.042432	0.0544332	0.0943679
			0.240					
			0.0671					
2018	0.414939	1285.86	0.1056	47371.77	19163.72	0.035343	0.0453392	0.0786021
			0.240					

Table 7. The comparison of analysis results in Y direction.

Code	Period (s)	Base shear (kN)	Displacement (m)	K_{elas} (kN/m)	K_{eff} (kN/m)	DL (m)	SD (m)	NC (m)
			0.0728					
1968	0.569467	414.16	0.1008	10951.24	5676.51	0.0230718	0.0295973	0.0513113
			0.240					
			0.0633					
1975	0.550027	497.07	0.1008	15773.69	7849.03	0.0218067	0.0279744	0.0484977
			0.240					
			0.0618					
1998	0.545897	592.37	0.096	20164.37	9587.37	0.043817	0.0562099	0.0974481
			0.240					
			0.082					
2007	0.530264	711.3	0.1392	21420.88	8673.52	0.0460447	0.0590677	0.1024025
			0.240					
			0.0731					
2018	0.414939	1243.29	0.1248	46356.85	17009.65	0.037526	0.0481396	0.083457
			0.240					

Table 8. Load factors, total support force and moments.

Code	X Direction				Y Direction			
	Total Support Force		Moment		Total Support Force		Moment	
	Load Factor	Total Support Force (kN)	Load Factor	Moment (kN·m)	Load Factor	Total Support Force (kN)	Load Factor	Moment (kN·m)
1968	4.15	414.163	4.096	845.394	4.151	414.163	3.745	844.957
1975	4.975	497.071	4.506	905.650	4.969	496.896	4.402	905.592
1998	5.933	592.373	5.157	1066.483	7.3741	733.06	6.7398	1319.594
2007	7.112	711.298	6.8787	1281.552	9.0158	901.587	8.8904	1579.939
2018	12.432	1243.393	12.373	2094.214	12.8585	1285.857	12.3514	2126.838

The comparison of the pushover curves obtained for the X and Y-direction by considering the minimum conditions regarded in the earthquake codes were given in Figs. 9 and 10, respectively.

The comparison of all values obtained as a result of dynamic time-history analysis for earthquake code was given in Table 9.

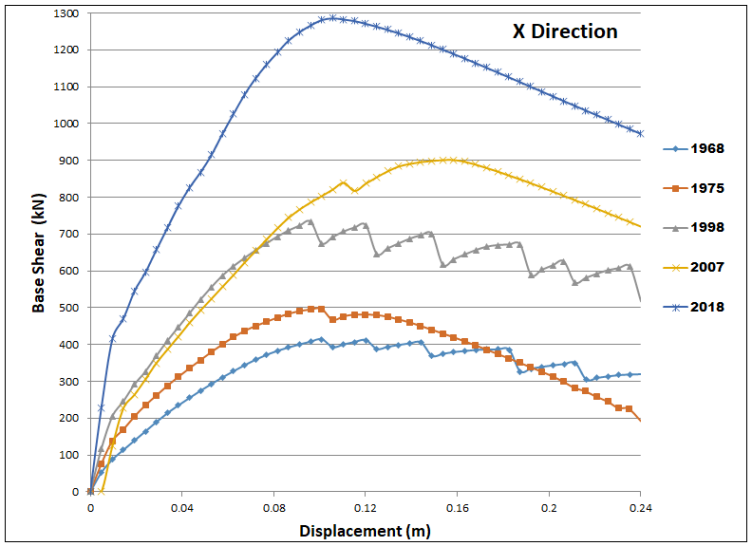

Fig. 9. The comparison of the pushover curves obtained for the X-direction.

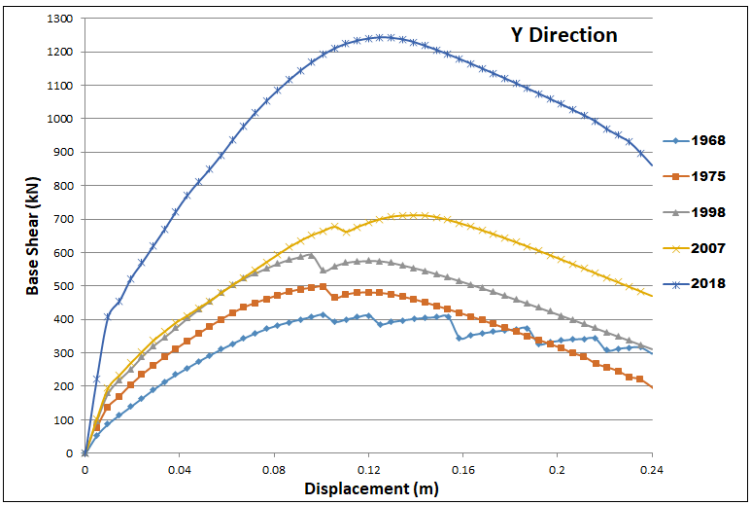

Fig. 10. The comparison of the pushover curves obtained for the Y-direction.

Table 9. The comparison of dynamic time-history analysis for different codes.

Code	Displacement (m)		Total Support Force (kN)		Total Support Moment (kNm)		Velocity (m/s²)		Global Mass Force (kN)		Hysteric Curve	
	Time (s)	N411	Time (s)	Value	Time (s)	Value	Time (s)	N411	Time (s)	Value	Displacement (m)	Base Shear (kN)
1968	2.35	0.043	2.43	260.6	2.43	544.20	2.64	0.350	2.43	260.16	0.202	260.581
1975	2.37	0.042	2.46	315.4	2.46	617.83	2.66	0.360	2.46	314.99	0.203	315.393
1998	2.37	0.041	2.47	358.2	2.47	980.20	2.67	0.343	2.47	357.61	0.203	358.214
2007	6.20	0.033	6.64	553.5	6.64	1062.13	8.19	0.393	6.64	552.81	0.424	553.456
2018	9.62	0.029	9.95	638.2	9.95	1177.37	9.50	0.315	9.95	637.95	0.627	638.203

Due to the minimum conditions that change within each updated code, the building period values have decreased. Accordingly, the stiffness values of the structure are increased. Therefore, every current code has suggested minimum conditions for more rigid structures. Each code increased the earthquake behaviour of the structures by designing structures with higher seismic capacity than the previous one. Moreover, the target displacement values are decreased with respect to each new code. The reason for this decrease is that more rigid structures are obtained for the variables that is used in this study. The period value is changed by 27% from the first codes to the last one. The change in the seismic capacity in the codes of 1968 and 2018 was calculated as approximately 200%. The variation in the stiffness values was quite high.

6. Conclusions

The earthquake damages and developing engineering technologies force governments to constantly update the rules of earthquake-resistant structural design. This situation is much more important in regions where it is inevitable to live with earthquakes in the world. It is observed that structures are effective in the majority of life and property losses after earthquakes. Therefore, to reduce the amount of damage that may occur in buildings during this unpreventable natural disaster event, it is essential to build earthquake-resistant buildings. There are a number of analyses and rules to make structures resistant to earthquakes. In the whole process from the design phase to the use of the building, the meticulous application of these rules is the most basic engineering process. In Turkey, which suffers earthquake-led severe losses, changes on different dates in earthquake codes have been inevitable. For example, the concrete grade has been increased to a higher level with each new code. In the 1975 code, the minimum concrete grade to be used was C14, while this grade has been determined as C25 in the latest regulation.

The comparisons are performed using three different analysis types by considering the minimum conditions given for columns-beams in each code. As a result of the eigenvalue analysis, the period values have taken lower values in each new seismic design code. The low period values show an increase in the stiffness of the structure. This situation is observed with the increase of both elastic and effective stiffness of buildings. The seismic design capacities have increased in every new code due to the increased dimension and grade of material. The base shear force calculated for the 2018 code increased approximately three times more than the 1968 code. The displacement values at the moment of yield have taken

lower values in each new code due to the base shear forces. This has been achieved compatibly between 1968-1975-1998 and 2007-2018. Compared to previous years, the main reason for the lack of compliance for 2007-2018 can be explained by the fact that the minimum reinforcement grade for 2007-2018 was S420.This situation is also valid for the target displacements estimated for performance criteria. There is an increase in load factors obtained for each changing code, total support force and total support moment.

Dynamic time-history analysis has clearly demonstrated that each new code increases the earthquake resistance of the building. In a much longer time, much fewer displacements were gained. This is an indication that the structures improve themselves in terms of their stiffness. For larger displacement values, seismic capacity values also increased. This is also valid for the values of the other parameters. A total harmony is obtained between the three different types of analysis. It is concluded that the change of minimum dimension and material properties are given for each new code improved the earthquake-resistant structural design.

In future studies, it can be examined in more detail whether these conditions are considered in the codes or they reflect the requirements. In addition, more detailed analyses can be carried out by taking into account the minimum and maximum values recommended for other structural elements. While performing these analyses, taking into account the different types of analysis in the codes will make the results more valuable. This and similar studies will be a source for future studies.

REFERENCES

ABYYHY-1968 (1968). Specification for Structures to be built in Disaster Areas. Ankara, Turkey. Retrieved from https://www.resmigazete.gov.tr/arsiv/12801.pdf

ABYYHY-1975 (1975). Specification for Structures to be built in Disaster Areas. Ankara, Turkey. Retrieved from https://web-dosya.csb.gov.tr/db/destek/icerikler/1_1_1975_deprem_yonetmel-g--20191127140243.pdf

ABYYHY-1998 (1998). Specification for Structures to be built in Disaster Areas. Ankara, Turkey. Retrieved from https://web-dosya.csb.gov.tr/db/destek/icerikler/1_2_1997_deprem_yonetmel-g--20191127140319.pdf

Aksoylu C, Arslan MH (2019a). Empirical evaluation of periodic calculations for frame+shear wall type of reinforced concrete buildings according to TEC-2019 Standard. *Uludağ University Journal of the Faculty of Engineering,* 24(3), 365-382.

Aksoylu C, Arslan MH (2019b). Çerçeve türü betonarme binaların periyod hesaplarının farklı ampirik bağıntılara göre irdelenmesi. *Bitlis Eren Üniversitesi Fen Bilimleri Dergisi*, 8(2), 569-581. (in Turkish)

Aksoylu C, Arslan MH (2021). 2007 ve 2019 deprem yönetmeliklerinde betonarme binalar için yer alan farklı deprem kuvveti hesaplama yöntemlerinin karşılaştırılmalı olarak irdelenmesi. *International Journal of Engineering Research and Development*, 13(2), 359-374. (in Turkish)

Aksoylu C, Mobark A, Arslan MH, Hakkı Erkan İ (2020). A comparative study on ASCE 7-16, TBEC-2018 and TEC-2007 for reinforced concrete buildings. *Revista de la Construcción,* 19(2), 282-305.

Alyamaç KE, Erdoğan AS (2005). Geçmişten günümüze afet yönetmelikleri ve uygulamada karşılaşılan tasarım hataları. *4th National Conference on Earthquake Engineering*, Kocaeli, Turkey.

Antoniou S, Pinho R (2003). Seismostruct–Seismic Analysis Program by Seismosoft. Technical Manual and User Manual.

Bozer A (2020). Comparison of spectral accelerations according to DBYBHY 2007 and TBDY 2018 earthquake codes. *Dicle Univercity Jounal of Engineering*, 11(1), 393-404.

Caglar N, Demir A, Ozturk H, Akkaya A (2015). A simple formulation for effective flexural stiffness of circular reinforced concrete columns. *Engineering Applications of Artificial Intelligence*, 38, 79-87.

Chopra, AK, Goel RK (2002). A modal pushover analysis procedure for estimating seismic demands for buildings. *Earthquake Engineering and Structural Dynamics,* 31(3), 561-582.

DBYYHY-2007 (2007). Turkish Earthquake Code. Ankara, Turkey. Retrieved from https://www.resmigazete.gov.tr/eskiler/2007/03/20070306-3-1.pdf

EN 1998-3 (2005). Eurocode-8: Design of Structures for Earthquake Resistance-Part 3: Assessment and Retrofitting of Buildings. European Committee for Standardization, Bruxelles, Belgium.

Eslami A, Ronagh HR (2014). Effect of elaborate plastic hinge definition on the pushover analysis of reinforced concrete buildings. *The Structural Design of Tall and Special Buildings*, 23(4), 254-271.

Estêvão JM, Oliveira CS (2015). A new analysis method for structural failure evaluation. *Engineering Failure Analysis*, 56, 573-584.

Fajfar P (1999). Capacity spectrum method based on inelastic demand spectra. *Earthquake Engineering and Structural Dynamics*, 28(9), 979-993.

Hadzima-Nyarko M, Pavic G, Lesic M (2016). Seismic vulnerability of older confined masonry buildings in Osijek, Croatia. *Earthquakes and Structures*, 11(4), 629-648.

Hadzima-Nyarko M, Kalman Sipos T (2017). Insights from existing earthquake loss assessment research in Croatia. *Earthquakes and Structures*, 13(4), 365-375.

Inel M, Meral E (2016). Seismic performance of RC buildings subjected to past earthquakes in Turkey. *Earthquakes and Structures,* 11(3), 483-503.

Isik E, Kutanis M (2015). Performance based assessment for existing residential buildings in Lake Van basin and seismicity of the region. *Earthquakes and Structures,* 9(4), 893-910.

Isik E (2016). Consistency of the rapid assessment method for reinforced concrete buildings. *Earthquakes and Structures*, 11(5), 873-885.

Işık E, Özdemir M (2017). Performance based assessment of steel frame structures by different material models. *International Journal of Steel Structures,* 17(3), 1021-1031.

Isik E, Isik MF, Bulbul MA (2017). Web based evaluation of earthquake damages for reinforced concrete buildings. *Earthquakes and Structures*, 13(4), 387-396.

Işık E, Büyüksaraç A, Ekinci YL, Aydın MC, Harirchian E (2020a). The effect of site-specific design spectrum on earthquake-building parameters: a case study from the Marmara Region (NW Turkey). *Applied Science*, 10(20), 7247.

Işık E, Karaşin İB, Demirci A, Büyüksaraç A (2020b). Seismic risk priorities of site and mid-rise RC buildings in Turkey. *Challenge Journal of Structural Mechanics*, 6(4), 191-203.

Işık E, Harirchian E, Bilgin H, Jadhav K (2021). The effect of material strength and discontinuity in RC structures according to different site-specific design spectra. *Research on Engineering Structures and Materials*, IN PRESS.

Jamadin A, Ibrahim Z, Jumaat MZ, Hosen MA (2020). Serviceability assessment of fatigued reinforced concrete structures using a dynamic response technique. *Journal of Materials Research and Technology,* 9(3), 4450-4458.

Karaca H, Oral M, Erbil M (2020). Comparison of 2007 and 2019 Turkish earthquake codes in terms of design of structures, a case study in Nigde. *Nigde Omer Halisdemir Univercity Journal of Engineering Sciences*, 9(2), 898-903.

Karasin İB, Işık E, Demirci A, Aydin MC (2020). The effect of site-specific design spectra for geographical location on reinforced-concrete structure performance. *Dicle Univercity Journal of Engineering*, 11(3), 1319-1330.

Kemaloğlu M (2015). Historical and legal development of disaster management in Turkey. *Akademik Bakış Dergisi*, 5, 126-147.

Keskin E, Bozdoğan KB (2018). Evaluation of 2007 and 2018 Turkish earthquake code for the province of Kirklareli. *Kirklareli University Journal of Engineering and Science*, 4(1), 74-90.

Koçer M, Nakipoğlu A, Öztürk B, Al-hagri MG, Arslan MH (2018). Deprem kuvvetine esas spektral ivme değerlerinin TBDY 2018 ve TDY 2007'ye göre karşilaştirilmasi. *Selcuk-Technic Journal*, 17(2), 43-58. (in Turkish)

Kutanis M, Boru EO, Işık E (2017). Alternative instrumentation schemes for the structural identification of the reinforced concrete field test structure by ambient vibration measurements. *KSCE Journal of Civil Engineering,* 21(5), 1793-1801.

Luo YF, Liu YP, Hu ZY, Xiong Z (2017). A new method for dynamic analysis of spatial lattice structures based on mode selection and mode construction techniques. *International Journal of Steel Structures*, 17(3), 1157-1170.

Mander JB, Priestley MJ, Park R (1988). Theoretical stress-strain model for confined concrete. *Journal of Structural Engineering*, 114(8), 1804-1826.

Menegotto M (1973). Method of analysis for cyclically loaded RC plane frames including changes in geometry and non-elastic behavior of elements under combined normal force and bending. *Proceedings of IABSE Symposium on Resistance and Ultimate Deformability of Structures Acted on by Well-Defined Repeated Loads,* 15-22.

Nikoo M, Hadzima-Nyarko M, Khademi F, ad Mohasseb S (2017). Estimation of fundamental period of reinforced concrete shear wall buildings using self-organization feature map. *Structural Engineerings and Mechanics*, 63(2), 237-249.

Öztürk M (2018). An evaluation about 2018 Turkey Building Earthquake Regulations and Turkey earthquake hazards map based on Central Anatolia Region. *Selcuk-Technic Journal*, 17(2)**,** 31-42.

Pinto PE, Franchin P (2011). Eurocode 8-Part 3: Assessment and retrofitting of buildings. *Proceedings of the Eurocode 8 Background and Applications, Dissemination of Information for Training*, Lisbon, Portugal.

SeismoStruct v7 (2018). A computer program for static and dynamic nonlinear analysis of framed structures. Seismosoft. https://seismosoft.com/

TBDY-2018 (2018). Turkey Building Earthquake Regulation. Ankara, Turkey. Retrieved from https://www.resmigazete.gov.tr/eskiler/2018/03/20180318M1-2-1.pdf

Ugalde D, Lopez-Garcia D, Parra PF (2020). Fragility-based analysis of the influence of effective stiffness of reinforced concrete members in shear wall buildings. *Bulletin of Earthquake Engineering*, 18(5), 2061-2082.

Vibration Data (2020). http://www.vibrationdata.com/elcentro.htm (Access date: 02.01.2020).

Wilding BV, Beyer K (2018). The effective stiffness of modern unreinforced masonry walls. *Earthquake Engineering and Structural Dynamics,* 47(8), 1683-1705.

Xian L, He Z, Ou X (2016). Incorporation of collapse safety margin into direct earthquake loss estimate. *Earthquakes and Structures*, 10(2), 429-450.

Yakut A (2004). Preliminary seismic performance assessment procedure for existing RC buildings. *Engineering Structures,* 26(10), 1447-1461.

Zuo Y, Zha X (2018). FEM and experimental study on mechanical property of integrated container building. *International Journal of Steel Structures*, 18(2), 699-718.

Challenge Journal of Structural Mechanics

Research Article

Investigation of moment-curvature and effective section stiffness of reinforced concrete columns

Saeid Foroughi [a,*], S. Bahadır Yüksel [a]

[a] *Department of Civil Engineering, Konya Technical University, 42250 Konya, Turkey*

ABSTRACT

In determining the seismic performance of reinforced concrete (RC) structures in national and international seismic code, it is desired to use effective section stiffness of the cracked section in RC structural elements during the design phase. Although the effective stiffness of the cracked section is not constant, it depends on parameters such as the dimension of the cross-section, concrete strength and axial force acting on the section. In this study, RC column models with different axial load levels, concrete strength, longitudinal and transverse reinforcement ratios were designed to investigate effective stiffness. Analytically investigated parameters were calculated from TBEC (2018), ACI318 (2014), ASCE/SEI41 (2017), Eurocode 2 (2004) and Eurocode8 (2004, 2005) regulations and moment-curvature relationships. From the numerical analysis results, it is obtained that the axial load level, concrete strength, longitudinal and transverse reinforcement ratios have an influence on the effective stiffness factor of RC column sections. The calculated effective stiffness for RC columns increases with increasing transverse reinforcement ratio, longitudinal reinforcement ratio and concrete strength. Due to the increase of axial force, effective stiffness values of concrete have increased.

ARTICLE INFO

Article history:
Received 30 April 2021
Revised 14 June 2021
Accepted 7 July 2021

Keywords:
Columns
Seismic performance
Seismic codes
Effective stiffness
Moment-curvature

1. Introduction

Reinforced concrete (RC) columns are the critical members of moment-resisting structural systems and have to be designed adequately in strength and ductility (Yüksel and Foroughi, 2019). Usually, it is desirable to design a (RC) member with sufficient curvature ductility capacity to avoid brittle failure in flexure and to insure ductile behavior, especially under seismic conditions (Foroughi and Yüksel, 2020). The correct estimate of curvature ductility and effective stiffness of (RC) members has always been an attractive subject of study as it engenders a reliable estimate of the capacity of buildings under seismic loads (Foroughi et al., 2020). It is generally accepted that, in the interest of safety, it is essential to provide a minimum level of flexural ductility, which will allow energy dissipation and moment redistribution as required (Baji and Ronagh, 2015). The moment-curvature relation for simple bending is a well-studied subject and the classical moment-curvature diagram is commonly found in the literature (Petschke et al., 2013). The flexural response is usually calculated with a numerically-based moment-curvature diagram of the base section and equivalent plastic hinge length (Gentile and Raffaele, 2018).

Seismic analysis and design of RC structures are performed based on linear behavior. However, taking into account the effect of cracking under severe earthquakes, nonlinear analysis is performed (Pique and Burgos 2008). Cracked section properties must be used for the analysis of existing structures. Cracked section properties may also be used when performing advanced analyses (Wong et al. 2017). Cracks in concrete, which reduce the stiffness of (RC) members, occur at loads much smaller than those corresponding to the yielding of the reinforcement and bearing capacity of the members (Vidović et al., 2012). Concrete cracking reduces the bending and shear stiffness of (RC) members. Therefore,

* *Corresponding author*. E-mail address: saeid.foroughi@yahoo.com (S. Foroughi)
ISSN: 2149-8024 / DOI: https://doi.org/10.20528/cjsmec.2021.03.003

analyzing (RC) structures without considering the cracking effect may not represent the actual behavior (Çağlar et al., 2015). The effective flexural stiffness EI of the column represents the equivalent stiffness of a fictitious column with constant stiffness, whose effective buckling length and critical axial load agree with those of the real column (Bonet et al., 2011).

Various research studies have been conducted on the effective stiffness of RC structural members. In the studies on the effective section stiffnesses, the equations proposed for the design were investigated by considering the parameters affecting the bending stiffness of the columns. The researchers proposed equations for the examination of the effective section stiffnesses of (RC) columns, taking into account different parameters and section properties. Various parameters such as the axial load level, the eccentricity of the axial load and the effect of the longitudinal reinforcement, the normal and high strength concrete, the concrete compressive strength and the reinforcement ratio were taken into account (Avşar et al., 2014; Kumar and Singh, 2010; Elwood and Eberhard, 2009; Khuntia and Ghosh, 2004; Mehanny et al., 2001; Panagiotakos and Fardis, 2001; Paulay and Priestley, 1992; Mirza, 1990).

Current design codes and technical recommendations often provide rough indications on how to assess effective stiffness of RC frames subjected to seismic loads, which is a key factor when a linear analysis is performed (Micelli et al., 2015). In widely used codes and guidelines, the effective stiffness of (RC) members is expressed as a proportion of their stiffness, calculated on the basis of the cross-section properties. Several procedures are suggested to consider effective stiffness: Turkish Building Earthquake Code (TBEC, 2018), American Concrete Institute (ACI318, 2014), Seismic Evaluation and Retrofit of Existing Buildings (ASCE/SEI41, 2017), Design of Concrete Structures (Eurocode 2, 2004), Design of Structures for Earthquake Resistance (Eurocode 8, 2004) and Eurocode 8-Part 3: Assessment and Retrofitting of Buildings (Eurocode 8, 2005). The effective section stiffnesses of (RC) columns according to different parameters were calculated and compared according to the mentioned methods and codes. Analytically investigated parameters were calculated from different earthquake regulations, various procedures recommended by researchers and moment-curvature relationships. In this study, a simple formula as a securer, quicker and more robust is proposed to determine the effective flexural stiffness of cracked sections of RC columns. The effective stiffness of RC columns is obtained by based moment-curvature analyses depending on member properties such as axial load levels ($N/N_{max} = N/A_c f_{ck}$), concrete compressive strength (f_{ck}), longitudinal reinforcement ratio (ρ_s) and transverse reinforcement ratios (ρ_{st}). The analysis results obtained for different RC column models are examined by summarizing in graphs. The results obtained at the end were examined by comparing them according to different parameters and models.

2. Effective Section Stiffness of RC Column Elements

2.1. Effective section stiffness coefficient according to moment-curvature relations

The flexural stiffness affects the load-bearing capacity of the structural element. One of the realistic ways to calculate the effective section stiffnesses of reinforced concrete sections is to use moment-curvature relations. The effective stiffness does not reflect only the effect of cracking but also the state of the RC members determined from moment-curvature relationships. Effective stiffness (EI_e) of the cracked section in RC sections is determined by the ratio corresponding to the yield moment (M_y) and the yield curve ($\emptyset_y$), taking into account the moment-curvature relationship ($EI_e = M_y/\emptyset_y$). The stiffness of the uncracked section (EI) is calculated according to the gross moments of inertia (I) of the RC elements and the modulus of elasticity of the concrete (E_c). For concrete classes, concrete elasticity modulus ($E_c = 3250\sqrt{f_{ck}} + 14000\ MPa$) are calculated according to the concrete compressive strengths (f_{ck}) given in Requirements for Design and Construction of RC Structures (Turkish Standard-TS500, 2000). Effective stiffness coefficient of (RC) elements; it is calculated as $k_e = EI_e/EI$.

2.2. Effective section stiffness coefficient proposed in TBEC (2018)

Effective cross-sectional stiffness multipliers will only be applied to calculations that are included in earthquake-effect load combinations and under loads entered into these combinations. TBEC (2018) specifies the effective stiffness coefficient for the RC columns is specified as 0.7. Effective cross-sectional stiffnesses (EI) of the RC members designed according to the lumped plastic behavior will be determined according to Eq. (1), where M_y is the yield moment, θ_y is the chord rotation at the yielding end and L_s is the shear span. Shear span can be taken as approximately half of the span length of the columns. For the nonlinear calculation, chord rotation at the yielding (θ_y) of the RC members is calculated by Eq. (2). In the equation; f_{ye} is the expected yield strength of transverse reinforcement (f_{ye}=1.2f_{yk}) and f_{ce} expected compressive strength of concrete (f_{ce}=1.3f_{ck}), h is the section height, d_b is the longitudinal reinforcement diameter and $\emptyset_y$ is the yield curvature. $\eta = 1$ in columns.

$$(EI)_e = \frac{M_y}{\theta_y}\frac{L_s}{3} \tag{1}$$

$$\theta_y = \frac{\emptyset_y L_s}{3} + 0.0015\,\eta\left(1 + 1.5\frac{h}{L_s}\right) + \frac{\emptyset_y d_b f_{ye}}{8\sqrt{f_{ce}}} \tag{1}$$

2.3. Effective section stiffness coefficient proposed in ASCE standard (2017)

In ASCE/SEI-41 (2017), EI_{eff} for columns with a design gravity load less than $0.1A_g f_c$, EI_{eff} is specified as $0.3E_c I_g$. For columns with a compressive force greater than $0.5A_g f_c$, this coefficient is given as 0.7.

2.4. Effective section stiffness coefficient proposed in ACI standard (ACI 318, 2014)

In ACI318 (2014) specifies the effective stiffness for the RC columns is specified as $0.70E_cI_c$. Alternatively, the moments of inertia of compression members, I, shall be permitted to be computed as follow Eq. (3). I need not be taken less than $0.35I_g$ for the compression members. In the equation, A_{st} is the total area of longitudinal reinforcement, A_g is the gross area of concrete section, M_u is the factored moment at section, P_u is the factored axial force, P_o is the nominal axial strength and h is the height of members.

$$I = \left(0.80 + 25\frac{A_{st}}{A_g}\right)\left(1 - \frac{M_u}{P_u h} - 0.5\frac{P_u}{P_0}\right)I_g \leq 0.875I_g \quad (3)$$

2.5. Effective section stiffness coefficient proposed in Eurocode 8 (2005)

Part 3 of Eurocode 8 (2005) provides an equation based on moment-to-shear ratio and yield rotation, which can be used for the determination of a more accurate effective stiffness ($M_yL_v/3\theta_y$). The chord rotation at yielding θ_y, calculated at Eq. (4).

$$\theta_y = \Phi_y\frac{L_V + a_V z}{3} + 0.0014\left(1 + 1.5\frac{h}{L_V}\right) + \Phi_y\frac{d_{bL}f_y}{8\sqrt{f_c}} \quad (4)$$

$a_V z$ is the tension shift of the bending moment diagram; $z = d - d'$ in beam section; $\varepsilon_y = f_y/E_s$, d and d' are the depths to the tension and compression reinforcement, respectively; and d_{bL} is the diameter of the reinforcement. $a_V = 0$, if $V_{Rc} > M_y/L_s$ and $a_V = 1$, if $V_{Rc} \leq M_y/L_s$. $V_{R,c}$ is taken in accordance with 1992-1-1 (2004).

2.6. Effective section stiffness coefficient proposed in Eurocode 8 (2004)

In Eurocode 8 (2004), recommends that the elastic flexural and shear stiffness properties of concrete elements are taken as 50% of the corresponding stiffness of the uncracked element.

2.7. Effective section stiffness coefficient proposed in Eurocode2 (2004)

The following model may be used to estimate the nominal stiffness of slender compression members with arbitrary cross section:

$$EI = K_cE_{cd}I_c + K_sE_sI_s \quad (5)$$

where E_{cd} is the design value of the modulus of elasticity of concrete ($E_{cd} = E_{cm}/\gamma_{CE}$, the recommended γ_{CE} value is 1.2); I_c is the moment of inertia of concrete cross section; E_s is the design value of the modulus of elasticity of reinforcement; I_s is the second moment of area of reinforcement, about the centre of area of the concrete; K_c is a factor for effects of cracking, creep etc.; and K_s is a factor for contribution of reinforcement. As a simplified alternative, provided $\rho = A_s/A_c \geq 0.01$, the following factors may be used in Eq. (6). φ_{ef} is the effective creep ratio.

$$K_s = 0 \quad , \quad K_c = \frac{0.3}{(1+0.5\varphi_{ef})} \quad (6)$$

The stiffness should be based on an effective concrete modulus:

$$E_{cd,eff} = E_{cd}/(1 + \varphi_{ef}) \quad (7)$$

3. Material and Method

In determining the seismic performance of RC structures in national and international earthquake regulations, it is desired to use effective stiffness of the cracked cross-section in RC structural elements during the design phase. One of the realistic analyses of calculating the effective stiffness of RC structural members is the use of moment-curvature relations. Effective stiffness of the cracked cross-section in RC structural members are determined by the ratio of yield moment to yield curvature considering the moment-curvature relationship. The effective stiffness of the cracked cross-section depends on parameters such as structural member size, concrete strength and axial load levels. RC square and circular column models with different axial load levels, concrete strength, longitudinal and transverse reinforcement ratios were designed to investigate effective stiffness. The effective stiffness coefficient of the cracked cross-section of the RC structural members designed in different parameters were obtained analytically. Analytically investigated parameters were calculated from TBEC (2018), ACI318 (2014), ASCE/SEI41 (2017), Eurocode 2 (2004), Eurocode 8 (2004, 2005) regulations and moment-curvature relationships of cross-sections.

Reinforced concrete column models having different cross-sections were created in order to examine the effects of effective cross-sectional stiffness of design parameters of RC column cross-sections. In order to investigate the effect of axial load levels, longitudinal and transverse reinforcement ratio on the effective stiffness coefficient, the column models having dimensions of 500mm×500mm square cross-section and 600mm diameter circular cross-sections were designed. Six different longitudinal reinforcement (LR) diameters, two different transverse reinforcement (TR) diameters and three different transverse reinforcement spacing are used for each RC column model. In (RC) column models, longitudinal reinforcement diameters were selected as 20mm, 22mm, 24mm, 26mm, 28mm and 30mm. In (RC) column models, transverse reinforcement diameters; 10mm and 12mm and transverse reinforcement spacings; it was chosen as 50mm, 75mm and 100mm. The reinforcement ratios used in the RC columns cross-sections have been determined by considering the limitations given in TS500 (2000) and TBEC (2018). Details for the designed RC column cross-sections with different pa-

rameters are given in Table 1 and Fig. 1. Accurate calculation of moment-curvature relations of (RC) elements is a reliable indicator of the load capacity of structures subjected to seismic loads. It is essential for the calculation of cross-section strength, flexural stiffness and ductility, and for the nonlinear analysis of (RC) structures. Theoretical moment-curvature analysis for RC members indicating the available bending moment and curvature can be constructed providing that the stress-strain relations for both concrete and steel are known. Moment-curvature relationships were obtained by SAP2000 Software which takes the nonlinear behavior of materials into consideration. The combined effect of vertical and seismic loads (N_{dmax}), cross-section area of RC column shall satisfy the condition $A_c \geq N_{dmax}/0.4f_{ck}$. In this study, the moment-curvature relationships of the RC column cross-sections were investigated for the values of N/N_{max} ratios of 0.10, 0.20, 0.30 and 0.40. To investigate the effect of axial force on the cross-section behavior; the RC rectangular, square and circular columns were investigated under four different axial load levels. The designed RC columns are considered to be composed of three components; cover concrete, confined concrete and reinforcement steel. A confined and unconfined concrete model proposed by Mander et al. (1988) used to determine the moment-curvature relationships of RC members. In moment-curvature analyses, material models given in Fig. 2 are used for concrete and reinforcement steel. RC members having different geometries were designed considering the regulations of ACI318 (2014) and TBEC (2018). For all RC members, C30, C35, C40, C45 and C50 were chosen as concrete grade and B420C was selected as reinforcement for the reinforcement behavior model. In the moment-curvature analysis, the effect of concrete tensile strength is neglected because it is insignificant.

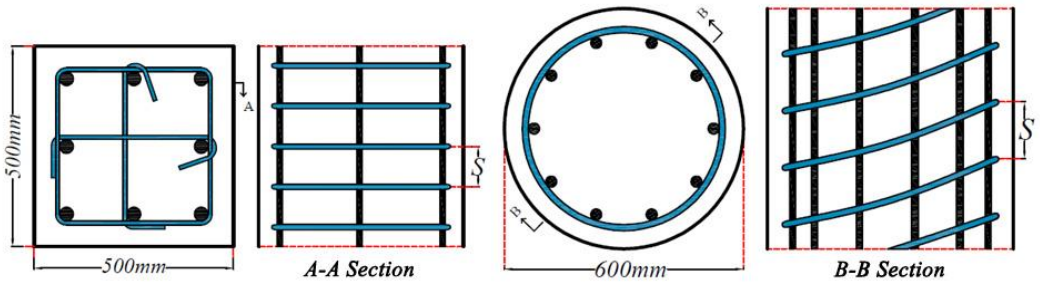

Fig. 1. Cross-sectional dimensions.

Table 1. Details for the designed RC column cross-sections.

Material	Longitudinal reinforcement	Transverse reinforcement		N/N_{max}
		Diameter	Spacing	
C30	Φ20mm	Φ10mm	50mm	0.10
C35	Φ22mm	Φ12mm	75mm	0.20
C40	Φ24mm		100mm	0.30
C45	Φ26mm			0.40
C50	Φ28mm			
	Φ30mm			

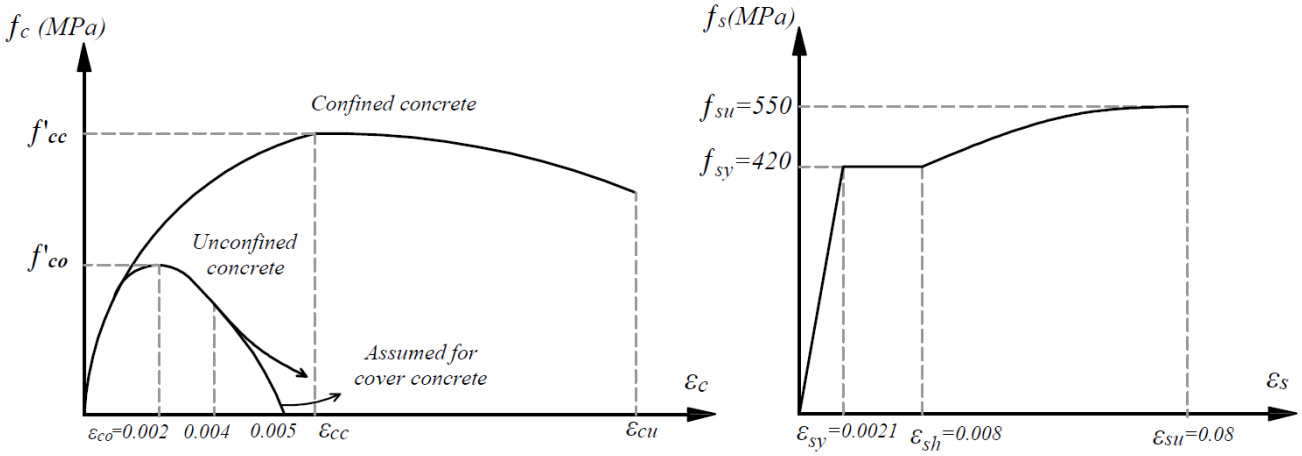

Fig. 2. Stress-strain relationships for concrete and reinforcement.

Analytically investigated parameters were calculated from different standards and codes and moment-curvature relationships of cross-sections. In this study, the effect of the axial load levels, concrete strength, longitudinal reinforcement and transverse reinforcement ratios were considered for square and circular RC column cross-sections. This study is based on parametric analysis of the cross-sectional response of a wide range of RC column cross-sections. The major factors affecting the effective stiffness of the RC column cross-sections are investigated. The effective section stiffness coefficient obtained from the analyses were compared with the effective cross-section stiffness coefficient given for RC columns in different regulations. The results of the comparison are examined in detail. The effective stiffness values obtained from the analysis results are presented in detail in the Research Findings and Discussion section.

4. Research Findings and Discussion

The effective flexural stiffness resulting from concrete cracking depends on some important parameters such as confinement, level of axial load, cross-section dimensions and material properties of concrete and reinforcement. The results of the parameters investigated for (RC) column models are summarized in the following sections according to cross-section geometries. The effective stiffness and effective stiffness coefficient of the cracked cross-section of the RC structural members designed in different parameters were obtained analytically. Analytically investigated parameters were calculated from TBEC (2018), ACI318 (2014), ASCE/SEI41 (2017), Eurocode2 (2004) and Eurocode8 (2004, 2005) regulations and moment-curvature relationships. The effective section stiffness coefficient obtained from the analyses were compared with the effective section stiffness coefficient given for RC square and circular columns in different regulations. The results obtained at the end were examined by comparing them according to different parameters and models.

4.1. Nonlinear moment-curvature analysis of reinforced concrete columns

In this part of the study, the moment-curvature relations are obtained by changing the axial load levels, concrete strength, longitudinal and transverse reinforcement ratio. A total of 1440 different analyzes were performed to determine the moment-curvature relationships and effective stiffness coefficients of square and circular (in two geometries) cross-section columns with different parameters. Each cross-sectional analysis is compared according to criteria which can change the effective stiffness of RC column cross-sections. The moment-curvature curves were drawn for different RC column models and were interpreted by comparing the curves. Moment (M_y, M_u) and curvature ($\emptyset_y$, $\emptyset_u$) values were calculated for yield and ultimate conditions from moment-curvature relationships according to different parameters in the designed (RC) square and circular column models (Figs. 3 and 4).

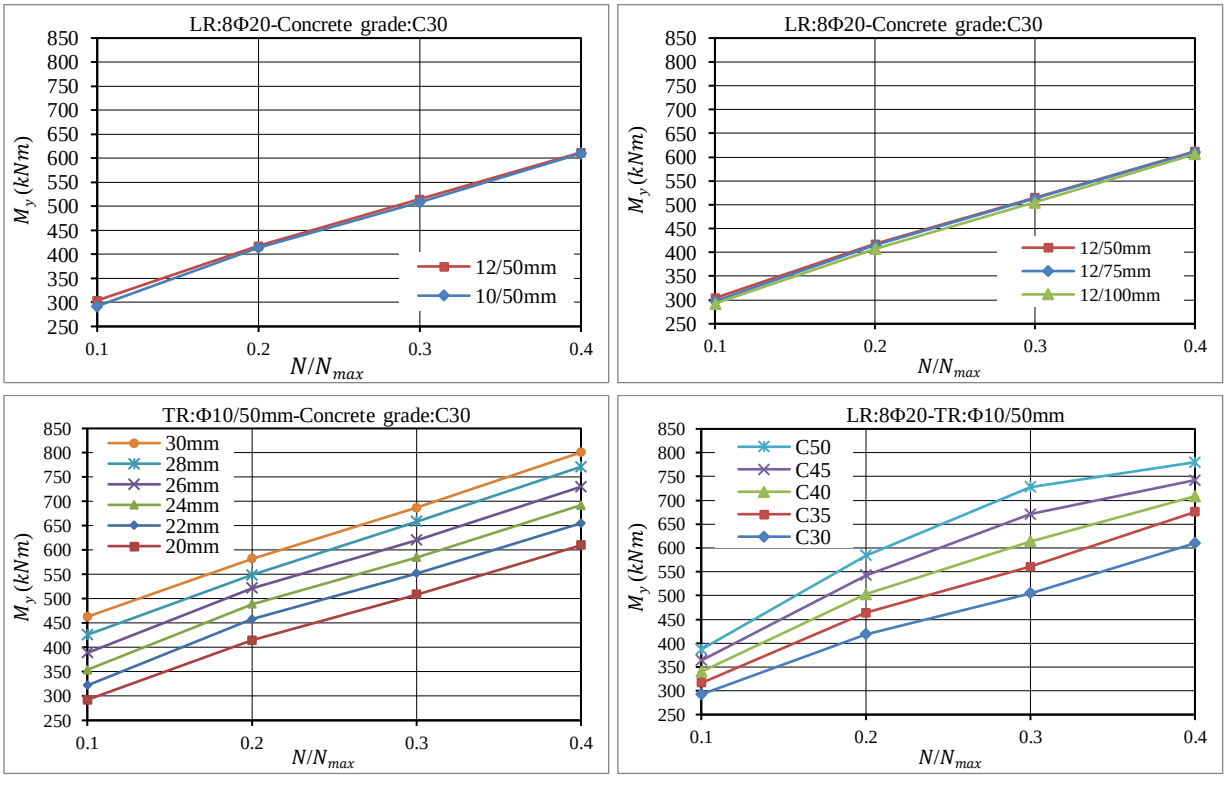

Fig. 3. (continued)

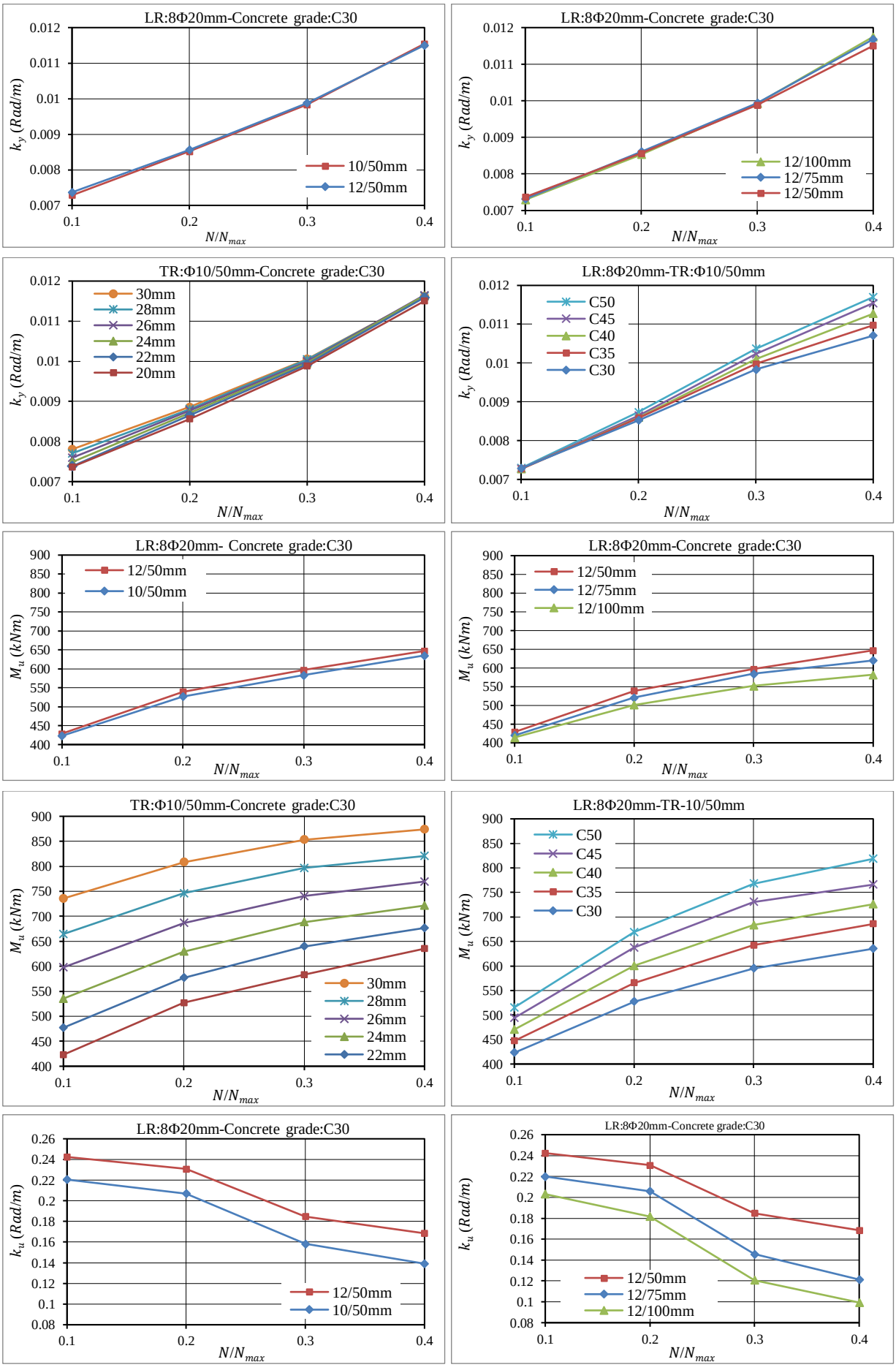

Fig. 3. (continued)

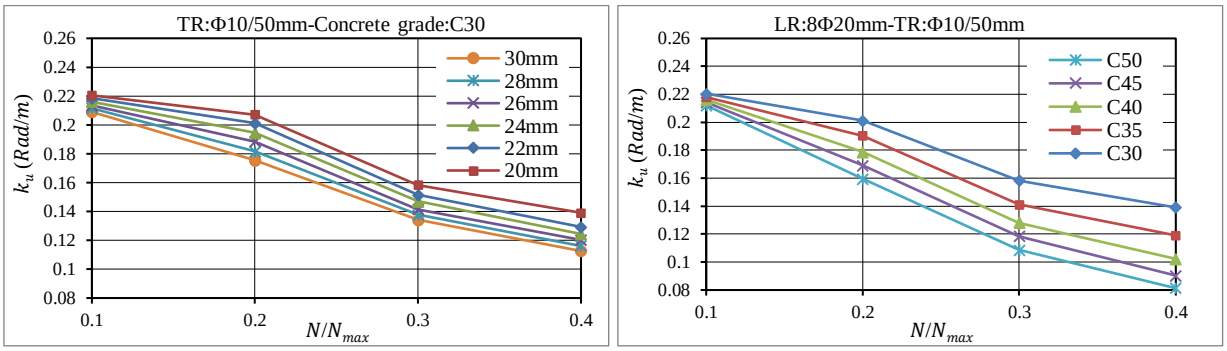

Fig. 3. Influence of N/N_{max}, concrete strength, longitudinal and transverse reinforcement on the moment-curvatures (square columns).

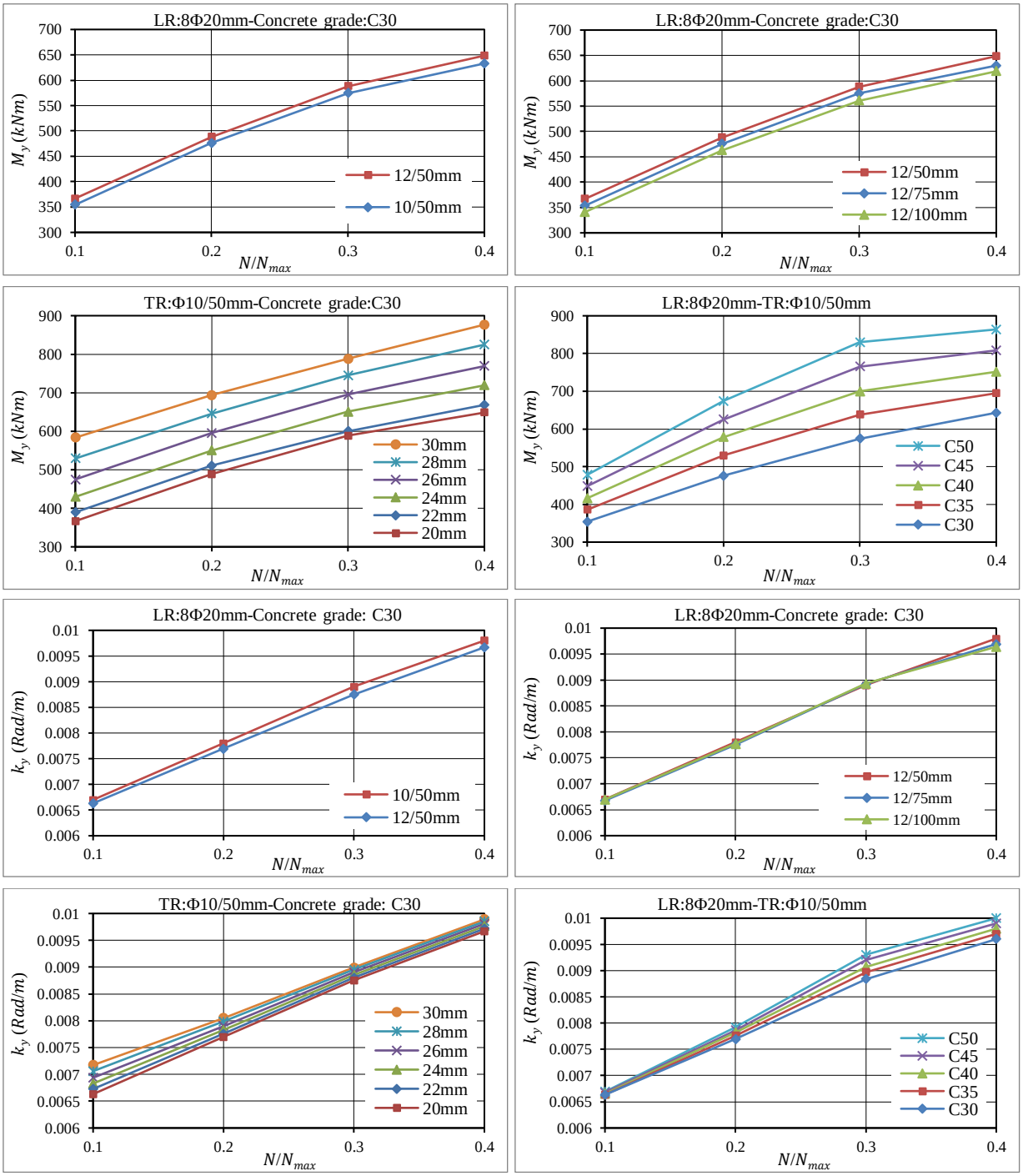

Fig. 4. (continued)

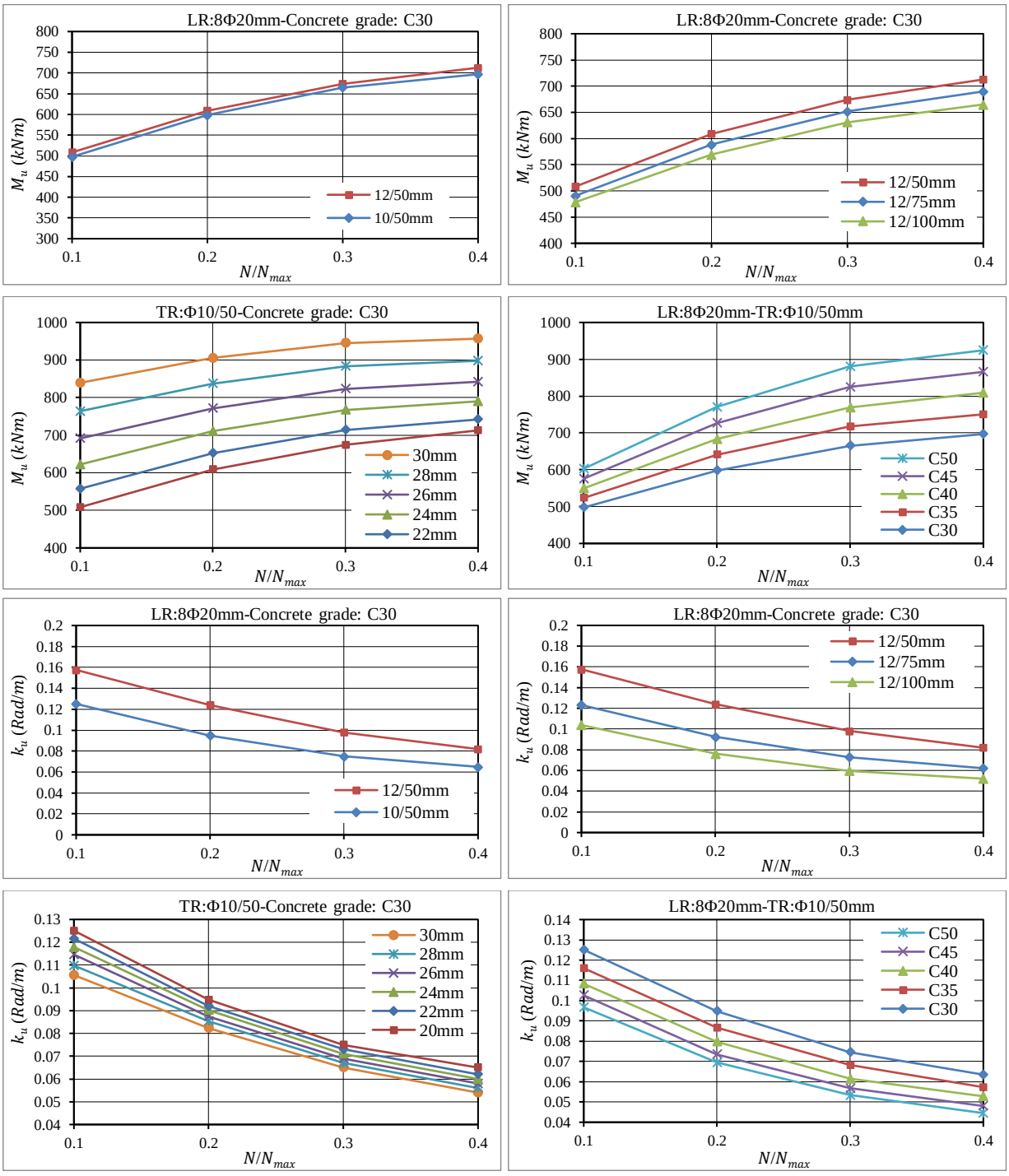

Fig. 4. Influence of N/N_{max}, concrete strength, longitudinal and transverse reinforcement on the moment-curvatures (circular columns).

4.2. Effective stiffness analysis of reinforced concrete columns

The effective stiffness coefficient of the (RC) square and circular column cross-sections designed according to different design parameters was investigated using the relationships proposed in different regulations and non-linear moment-curvature analysis. The effective stiffness of the RC columns is obtained by nonlinear moment-curvature analyzes depending on different design parameters. The effective stiffness coefficient obtained from analysis for different RC column models are examined by summarizing in graphs. The results obtained at the end were examined by comparing them according to different parameters (axial load, concrete compressive strength, longitudinal and transverse reinforcement ratio) and models (Square and circular cross-section). The effective stiffness coefficient obtained from the analyzes were compared from moment-curvature relations and different seismic codes (TBEC, 2018; ACI318, 2014; ASCE/SEI41, 2017; Eurocode 2, 2004; Eurocode 8, 2004; Eurocode 8-Part 3, 2005). The calculated effective stiffness coefficient are comparatively given in Figs. 5-17.

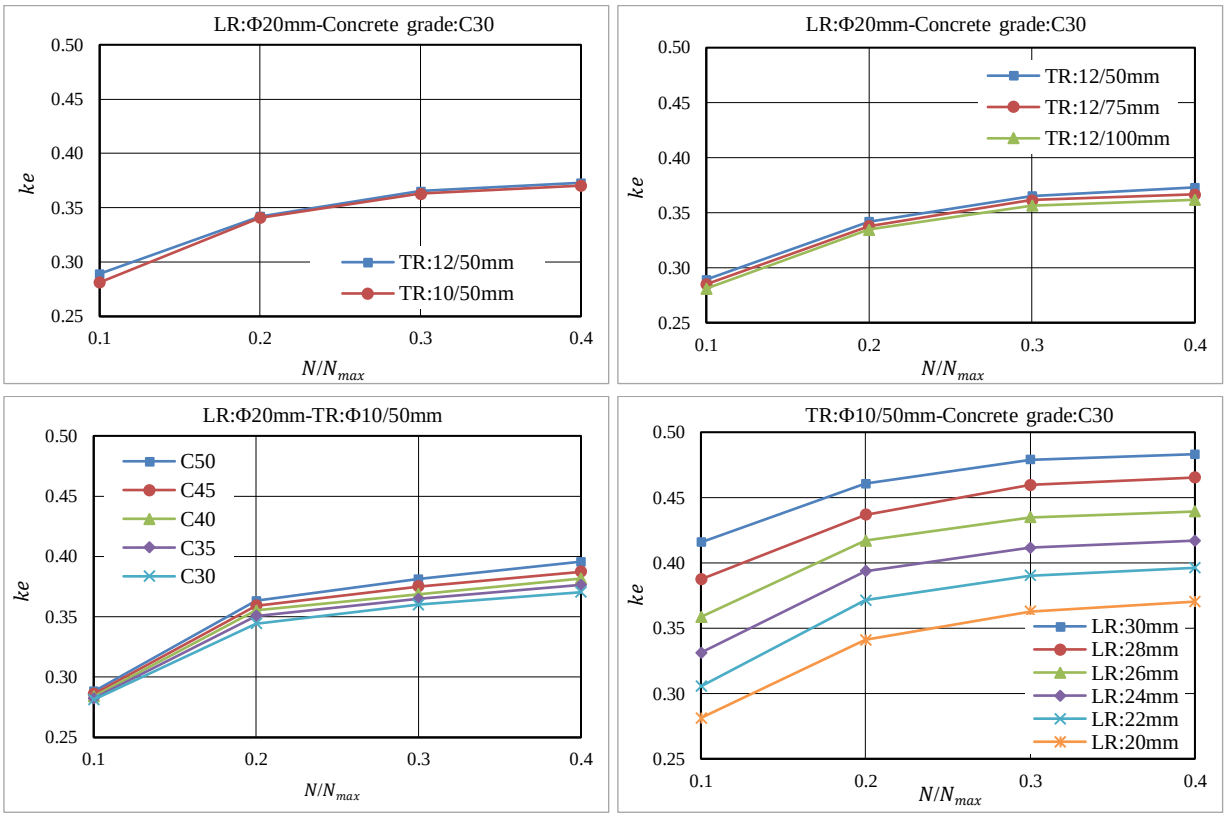

Fig. 5. k_e values obtained from moment-curvature relationships according to different parameters of the square column.

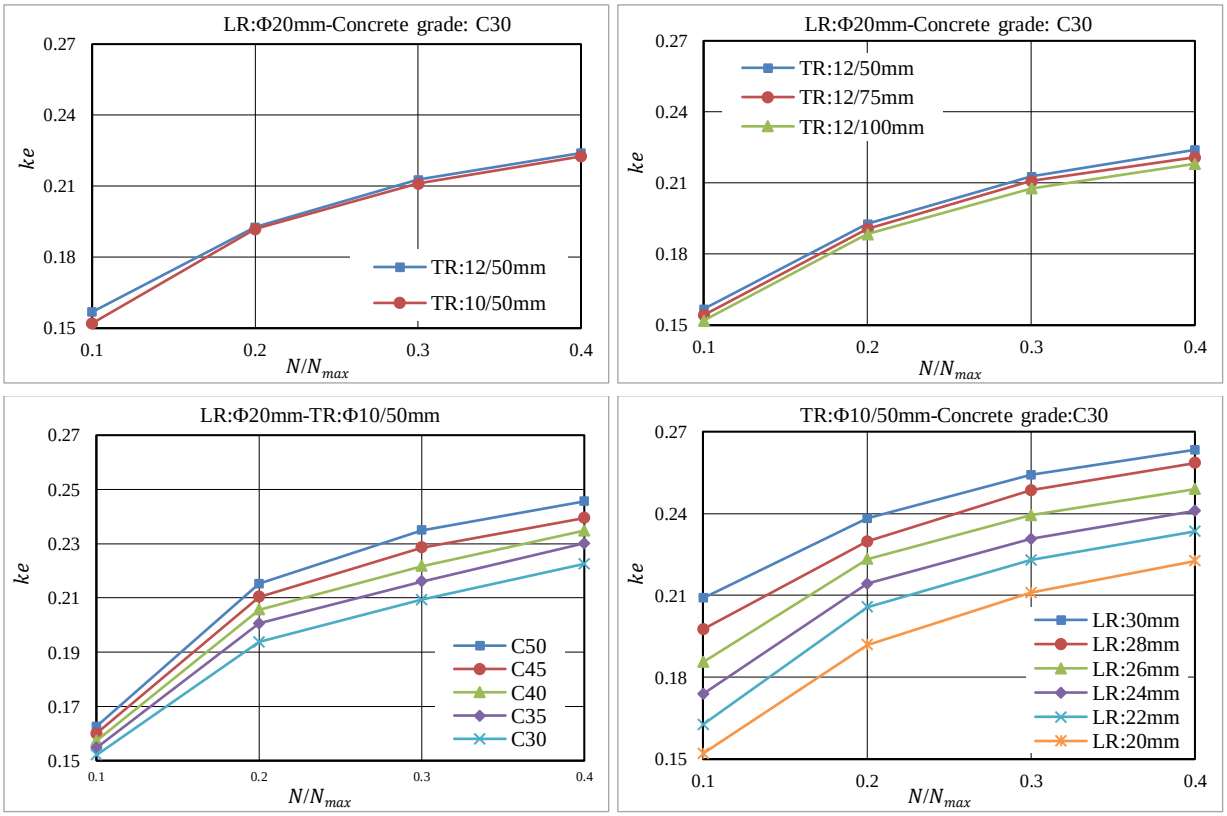

Fig. 6. k_e values obtained according to the non-linear behavior defined in TBEC (2018) of the square column.

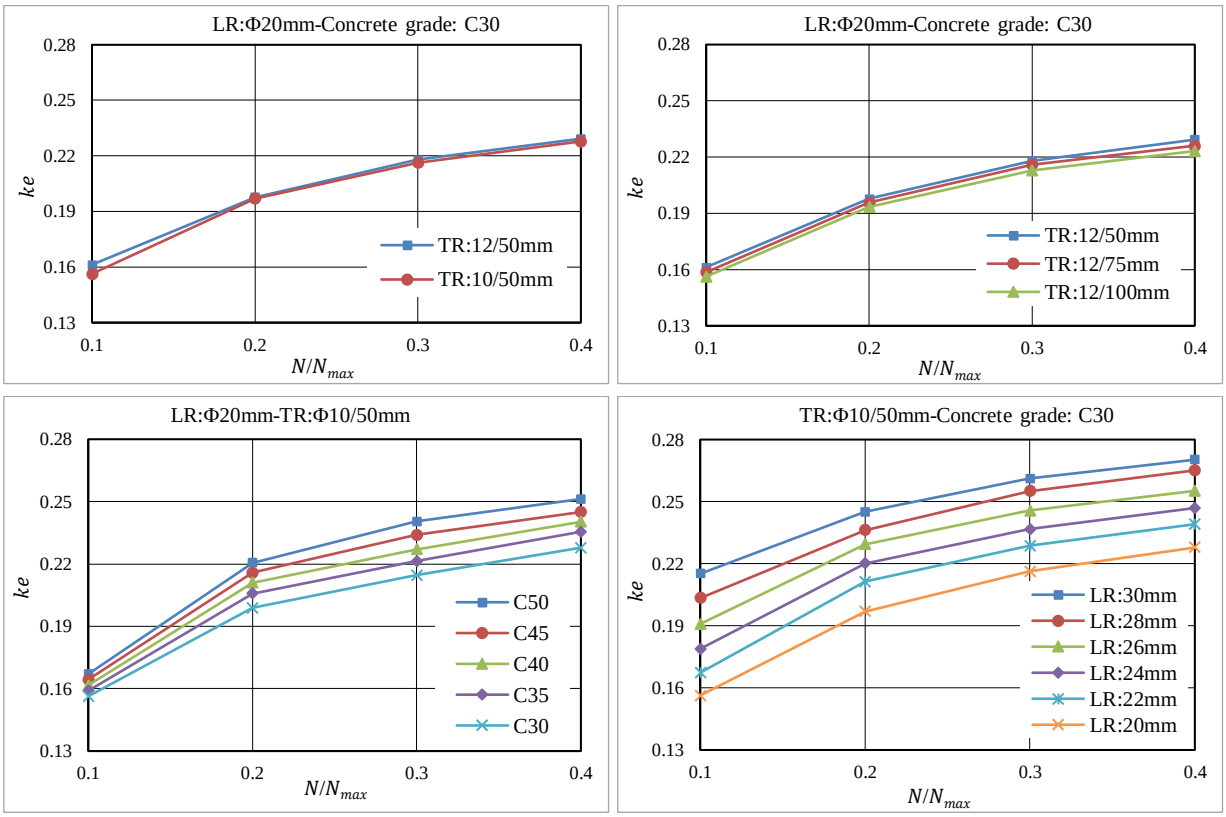

Fig. 7. k_e values obtained according to part 3 of Eurocode 8 (2005) of the square column.

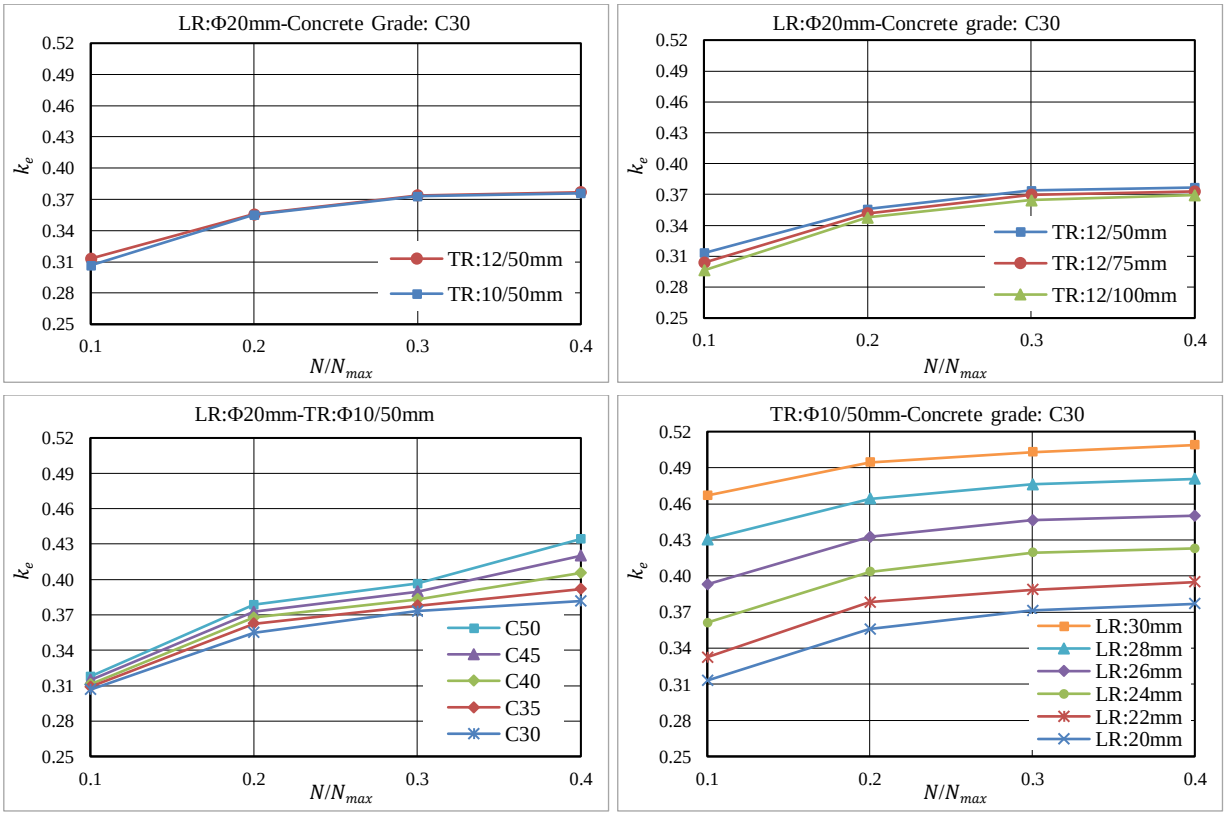

Fig. 8. k_e values obtained from moment-curvature relations according to different parameters of circular column.

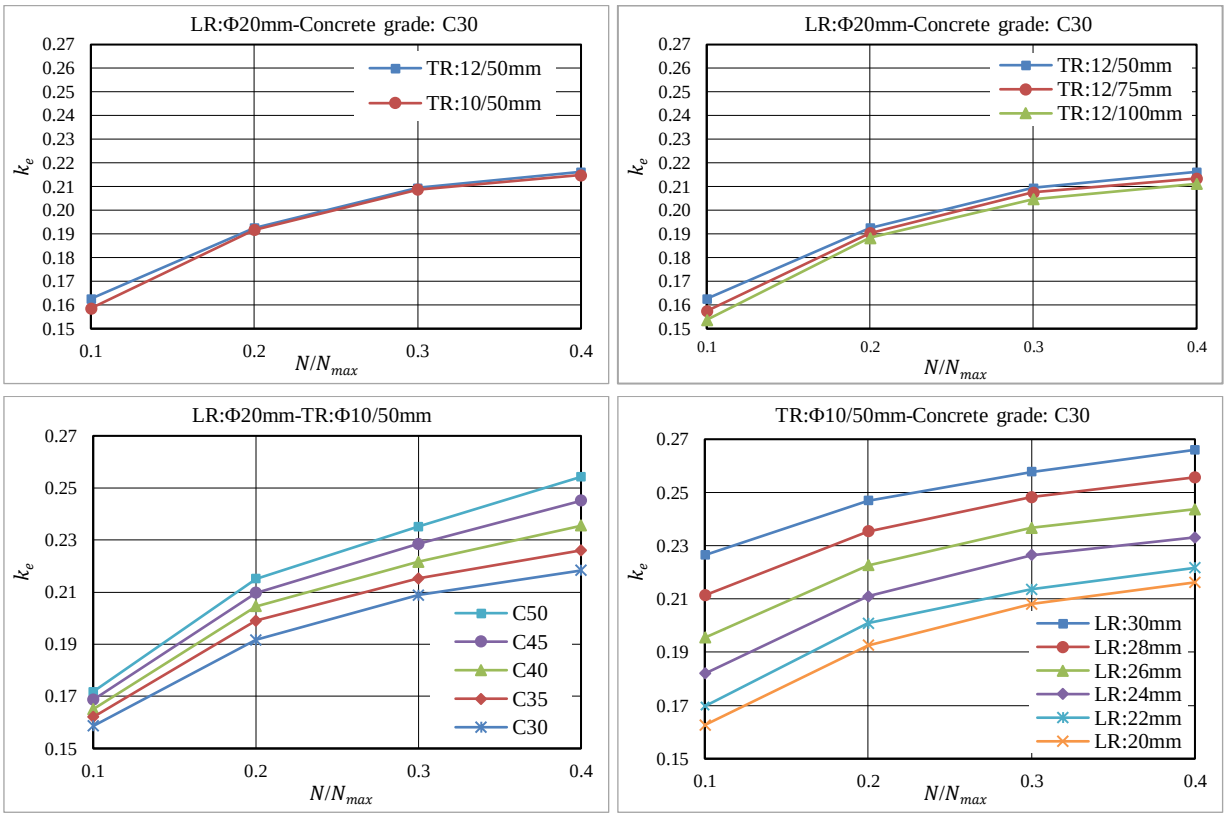

Fig. 9. k_e values obtained according to the non-linear behavior defined in TBEC (2018) of circular column.

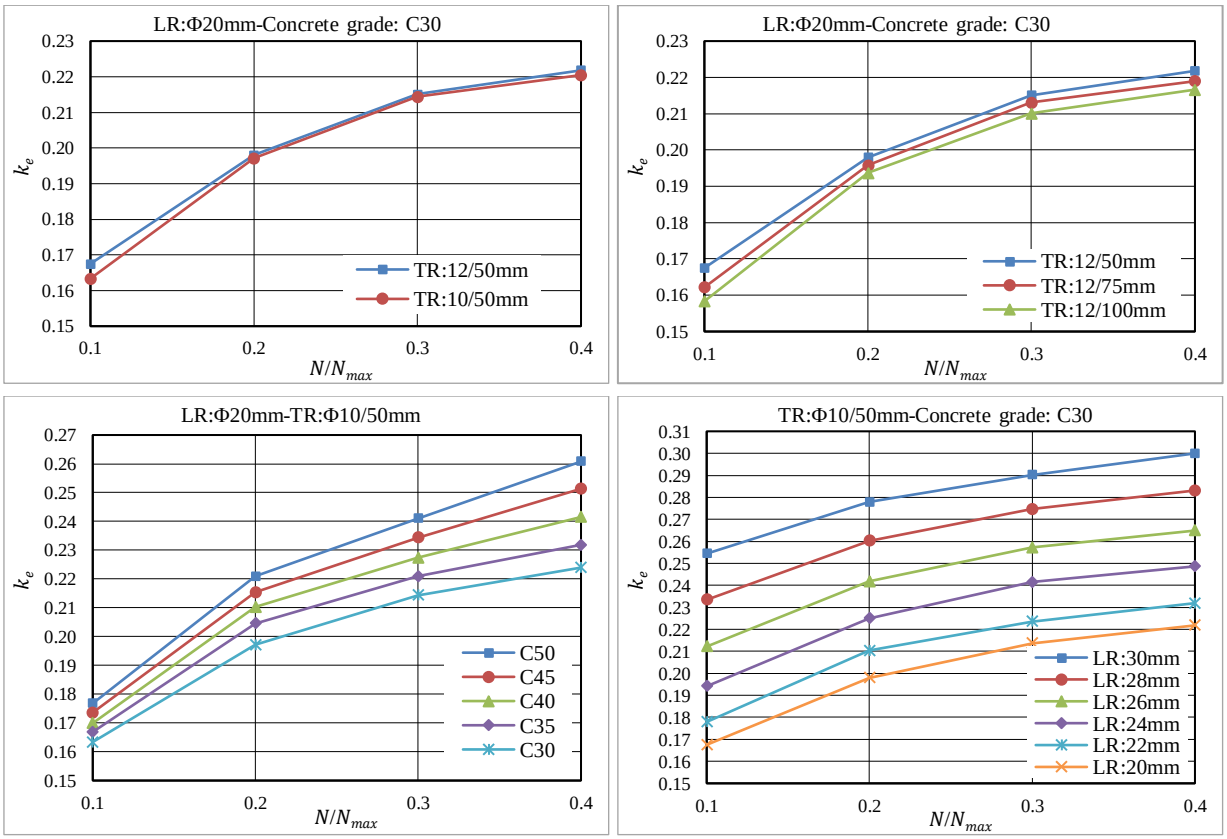

Fig. 10. k_e values obtained according to part 3 of Eurocode8 (2005) of circular column.

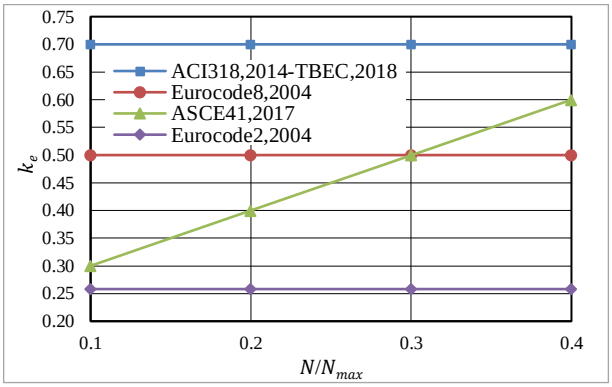

Fig. 11. k_e values obtained according to different seismic codes and standard of the columns.

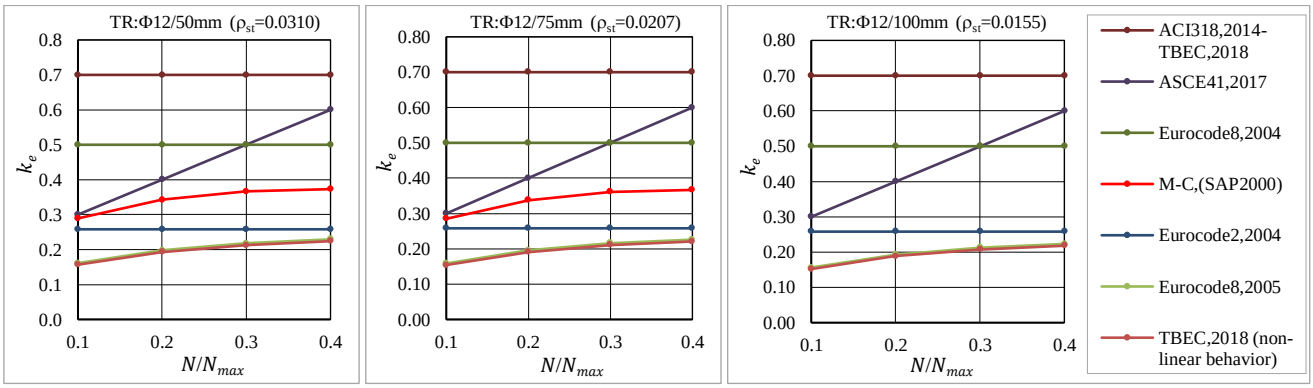

Fig. 12. Effect of transverse reinforcement on k_e of square column cross-sections (LR: Φ20mm-C30).

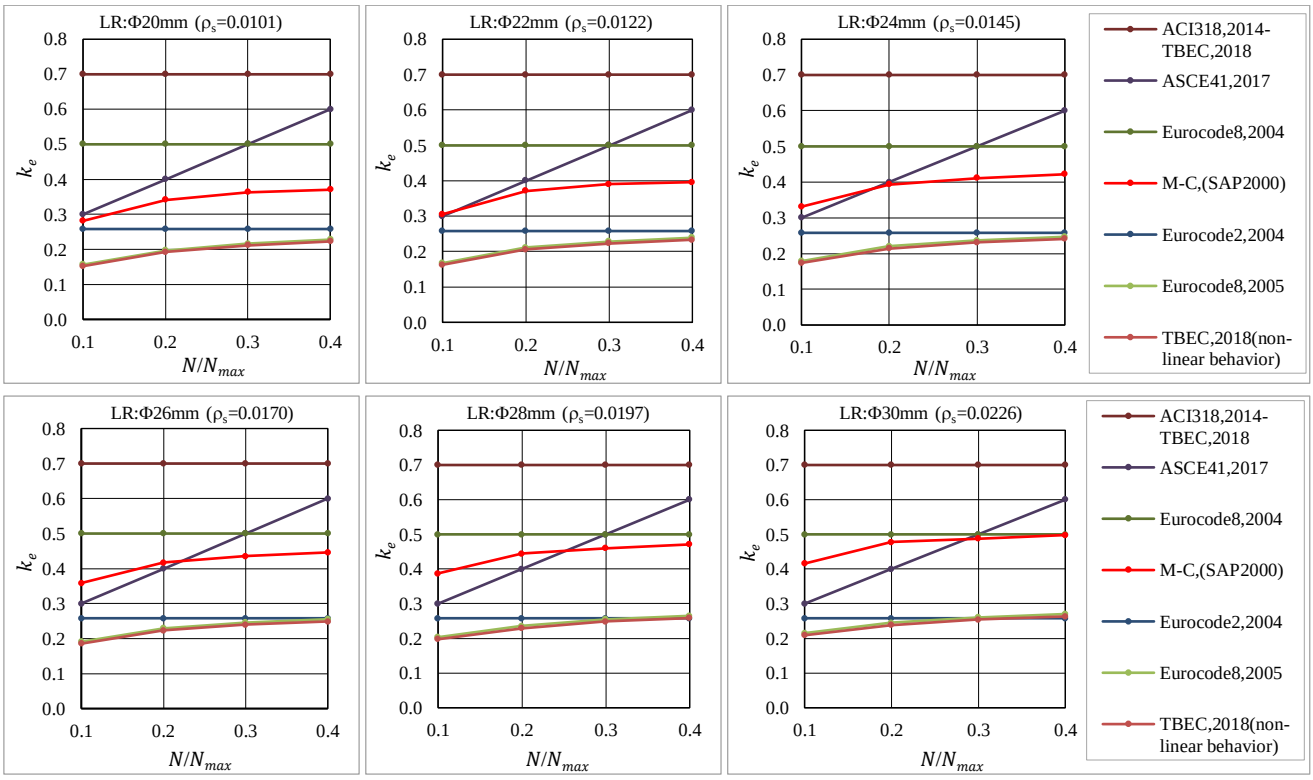

Fig. 13. Effect of longitudinal reinforcement on k_e of square column cross-sections (TR: Φ10/50mm-C30).

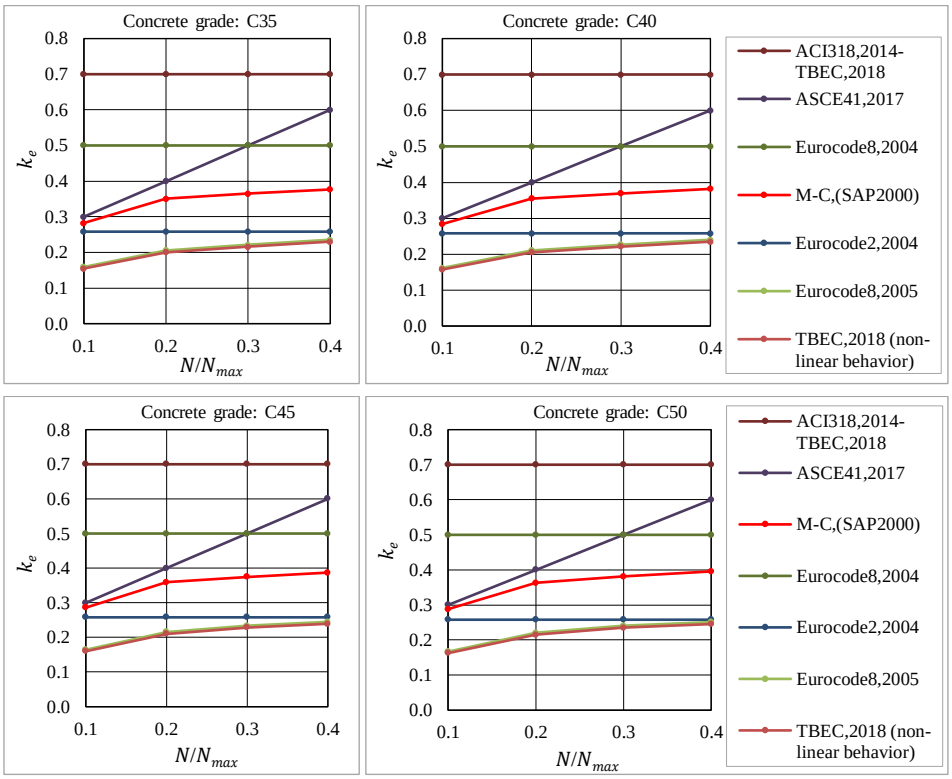

Fig. 14. Effect of concrete compressive strength on k_e of square column cross-sections (LR: Φ20mm, TR: Φ10/50mm).

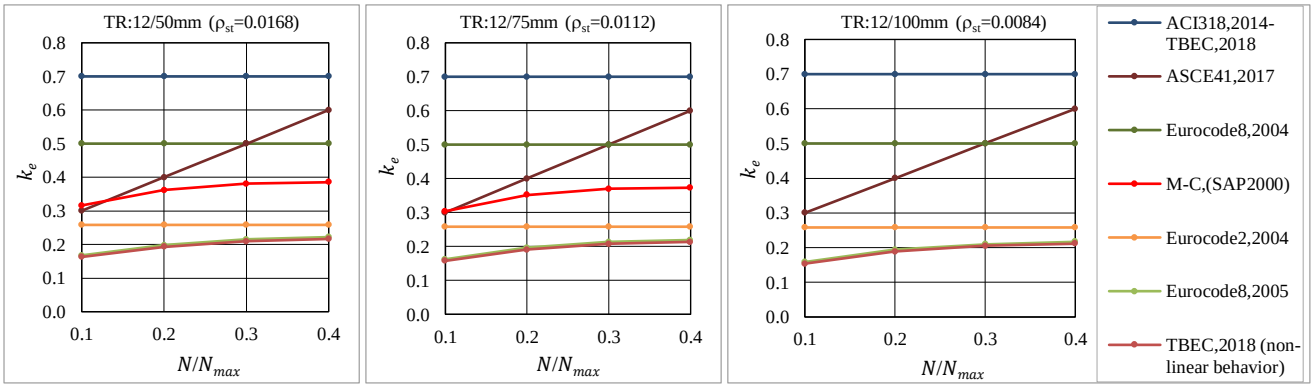

Fig. 15. Effect of transverse reinforcement on k_e of circular column cross-sections (LR: Φ20mm-C30).

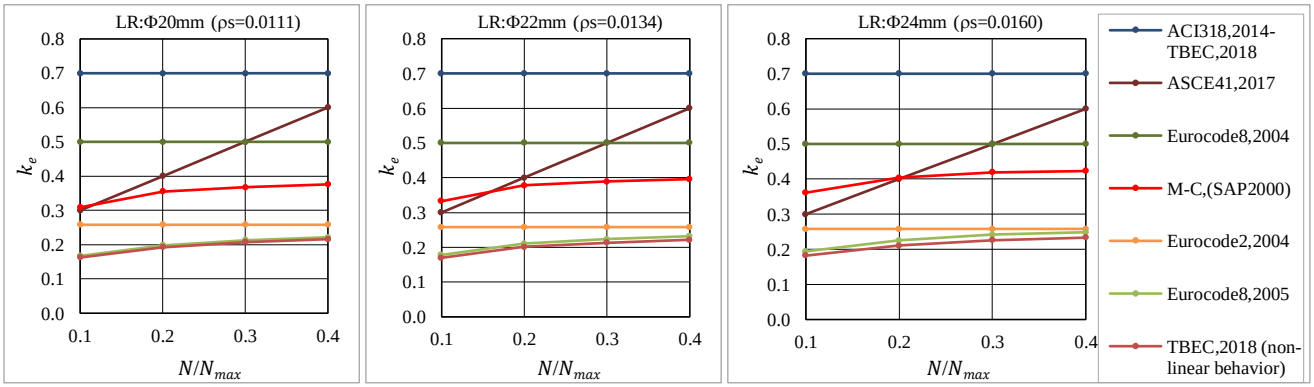

Fig. 16. (continued)

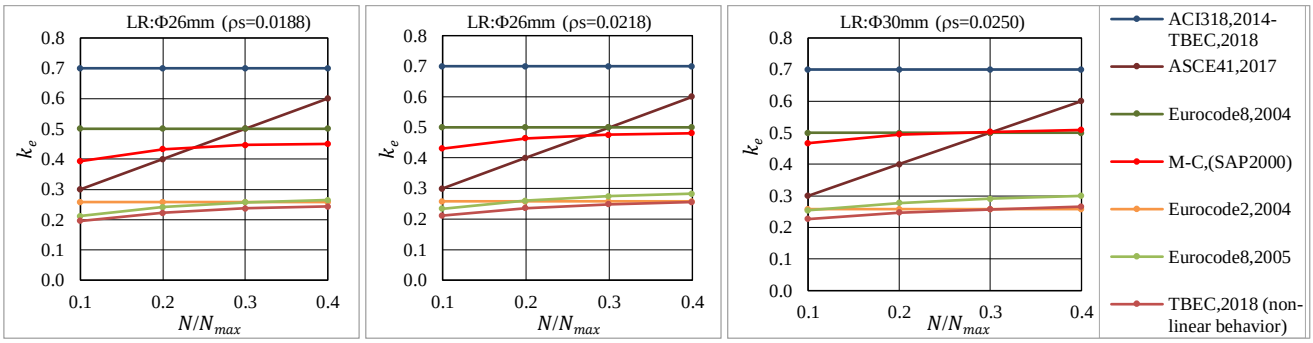

Fig. 16. Effect of longitudinal reinforcement on k_e of circular column cross-sections (TR: Φ10/50mm-C30).

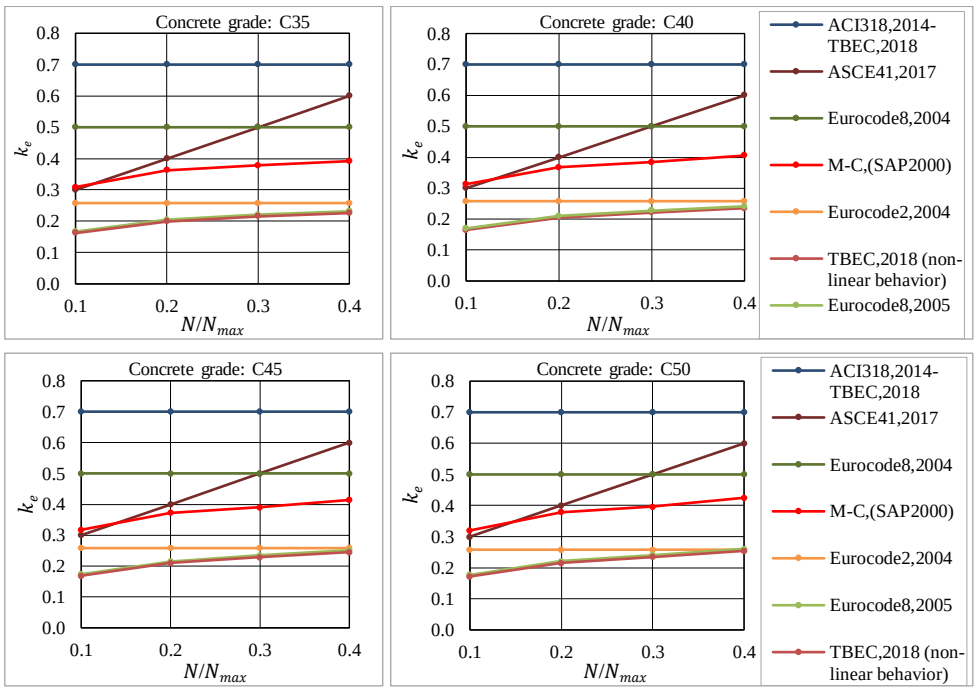

Fig. 17. Effect of concrete compressive strength on k_e of circular column cross-sections (LR: Φ20mm, TR: Φ10/50mm).

When the moment-curvature analysis results are examined, it is observed that the variation of the axial load, longitudinal reinforcement diameter, transverse reinforcement ratio have an important effect on the moment-curvature behavior of the (RC) columns. Yielding and ultimate moment capacities of the sections increase when the transverse reinforcement spacing decreases. The increase in the transverse reinforcement diameter increases the ultimate moment, ultimate curvature and curvature ductility values, but yield moment and yield curvature values remain almost constant. The increase in the axial load level causes curvature values to decrease. Yield and ultimate moment capacities of the members increase with the increment of longitudinal reinforcing ratio for the columns.

ACI318 (2014) gives a constant ratio of $0.70E_cI_c$ for columns. In ASCE/SEI-41 (2017), $f$or columns with a design gravity load less than $0.1A_gf_c$, EI_{eff} is specified as $0.3E_cI_g$. For columns with a compressive force greater than $0.5A_gf_c$, this coefficient is given as 0.7. The effective stiffness value of the cracked section given in Eurocode 8 (2004) is fixed. The effective stiffness of the cracked section is considered to be half of the initial stiffness. In Eurocode 8 (2004), features such as concrete strength, cross-section geometry, longitudinal and transverse reinforcement ratio and axial force acting on the cross-section are not taken into consideration. Part 3 of Eurocode 8 (2005) provides an equation based on moment-to-shear ratio and yield rotation, which can be used for the determination of a more accurate effective stiffness. Both the ultimate level and serviceability level loads are addressed in Eurocode 8 for linear and nonlinear analysis. According to Eurocode 2 (2004) in a second-order analysis based on stiffness, nominal values of the flexural stiffness should be used, taking into account the effects of cracking, material non-linearity and creep on the overall behavior. Similarly, in TBEC (2018), effective stiffness is assumed to be constant and effective stiffness coefficient values of the cracked section are 0.70 for the column. The effective stiffness of reinforced columns modelled according to the lumped plastic behavior in TBEC (2018) can be calculated depending on the effective yield moments, yield rotation and the shear span.

5. Conclusions

When the moment-curvature analysis results are examined, it is observed that the variation of the axial load, longitudinal reinforcement diameter, transverse reinforcement ratio have an important effect on the moment-curvature behavior of the (RC) columns. Yielding and ultimate moment capacities of the cross-sections increase when the transverse reinforcement spacing decreases. The ductile behavior for (RC) column cross-sections is observed due to the increment of curvature ductility with the increase of the transverse reinforcement ratio. The increase in the transverse reinforcement diameter increases the ultimate moment, ultimate curvature and curvature ductility values, but yield moment and yield curvature values remain almost constant (transverse reinforcement spacing and axial load levels are the constant). Yield moment, yield curvature, ultimate moment and ultimate curvature values increase however, curvature ductility values decrease as the longitudinal reinforcement diameter increases while other parameters kept constant. The increase in the axial load level causes curvature values to decrease. In cases where the axial load is low, (RC) cross-sections have a ductile behavior. Yield and ultimate moment capacities of the members increase with the increment of longitudinal reinforcing ratio for the columns cross-section.

In the relations suggested for the effective stiffness coefficient, the confining effect is not taken into account as in the regulations. Therefore, it means neglecting the effects of parameters such as cross-section dimension, concrete strength, confining effect and axial force acting on the cross-section. Determining the moment-curvature relationship in the design and evaluation of (RC) elements and obtaining effective stiffness values are of great importance in order to obtain more realistic results. Existing codes and previous studies revealed that the effective stiffness is often expressed in terms of the axial load level in the columns. The axial loads, concrete strength and the amount of longitudinal and transverse reinforcements have been identified as the most important factors affecting the cross-section yield point as well as the effective stiffness of the RC column cross-section. As can be seen from the comparison results, the effective stiffness values calculated from the SAP2000 program, from different regulations are different from each other. Taking the effective stiffness higher than the required value will cause the structural stiffness to be overestimated. As a result, problems will arise in the calculation and evaluation of structures. As can be seen from the comparison of effective stiffness coefficient values obtained with different regulations and relations for RC columns designed in different parameters; the calculated effective stiffness for RC columns increases with increasing transverse reinforcement ratio, longitudinal reinforcement ratio and concrete strength. Due to the increase of axial force, effective stiffness values of concrete have increased.

Acknowledgements

The authors thank the reviewers who evaluated the article for their time and valuable comments and suggestions.

References

ACI 318 (2014). Building Code Requirements for Reinforced Concrete and Commentary. American Concrete Institute Committee, USA.

ASCE/SEI41 (2017). Seismic Evaluation and Retrofit of Existing Buildings. The American Society of Civil Engineers, Reston, Virginia, p. 20191-4382, USA.

Baji H, Ronagh HR (2015). Probabilistic models for curvature ductility and moment redistribution of RC beams. *Computers and Concrete*, 16(2), 191-207.

Bonet JL, Romero ML, Miguel PF (2011). Effective flexural stiffness of slender reinforced concrete columns under axial forces and biaxial bending. *Engineering Structures*, 33(3), 881-893.

Çağlar N, Demir A, Ozturk H, Akkaya A (2015). A simple formulation for effective flexural stiffness of circular reinforced concrete columns. *Engineering Applications of Artificial Intelligence*, 38, 79-87.

Elwood KJ, Eberhard MO (2009). Effective Stiffness of Reinforced Concrete Columns. *ACI Structural Journal*, 106(4), 476-484.

Eurocode 2 (2004). Design of concrete structures: Part 1-1: General rules and rules for buildings, BS EN 1992-1-1:2004.

Eurocode 8 (2004). Design of structures for earthquake resistance: Part 1: General rules, seismic actions and rules for buildings, BS EN 1998-1:2004.

Eurocode 8 CEN (2005). Design of structures for earthquake resistance: Part 3: Assessment and retrofitting of buildings, BS EN 1998-3.

Foroughi S, Yuksel SB (2020). Investigation of the moment-curvature relationship for RC square columns. *Turkish Journal of Engineering (TUJE)*, 4(1), 36-46.

Foroughi S, Jamal R, Yüksel SB (2020). Effect of confining reinforcement and axial load level on curvature ductility and effective stiffness of reinforced concrete columns. *El-Cezerî Journal of Science and Engineering*, 7(3), 1309-1319.

Gentile R, Raffaele D (2018). Simplified analytical moment-curvature relationship for hollow circular RC cross-sections. *Earthquakes and Structures*, 15(4), 419-429.

Khuntia M, Ghosh SK (2004). Flexural stiffness of reinforced concrete columns and beams: analytical approach. *ACI Structural Journal*, 101(3), 351-363.

Kumar R, Singh Y (2010). Stiffness of reinforced concrete frame members for seismic analysis. *ACI Structural Journal*, 107(5), 607-615.

Mander JB, Priestley MJN, Park R (1988). Theoretical stress-strain model for confined concrete. *Journal of Structural Engineering*, 114(8), 1804-1826.

Mehanny SSF, Kuramoto H, Deierlein GG (2001). Stiffness modeling of RC beam-columns for frame analysis. *ACI Structural Journal*, 98(2), 215-225.

Micelli F, Candido L, Leone M, Maria AA (2015). Effective stiffness in regular R/C frames subjected to seismic loads. *Earthquakes and Structures*, 9(3), 481-501.

Mirza SA (1990). Flexural stiffness of rectangular RC columns. *ACI Structural Journal*, 87(4), 425-435.

Panagiotakos TB, Fardis MN (2001). Deformations of reinforced concrete members at yielding and ultimate. *ACI Structural Journal*, 98(2), 135-148.

Paulay T, Priestley MJN (1992). Seismic Design of Reinforced Concrete and Masonry Buildings. John Wiley & Sons, New York.

Petschke T, Corres H, Ezeberry JI, Pérez A, Recupero A (2013). Expanding the classic moment-curvature relation by a new perspective onto its axial strain. *Computers and Concrete*, 11(6), 515-529.

Pique JR, Burgos M (2008). Effective stiffness of reinforced concrete elements in seismic analysis and design. *The 14th World Conference on Earthquake Engineering,* 12-17 October, Beijing, China.

SAP (2000). Structural Software for Analysis and Design. Computers and Structures, Inc, USA.

TBEC (2018) Turkish Building Earthquake Code: Specifications for Building Design under Earthquake Effects, T.C. Ministry of Environment and Urbanization, Ankara, Turkey.

TS500 (2000) Requirements for Design and Construction of Reinforced Concrete Structures. Turkish Standards Institute, Ankara, Turkey.

Vidović D, Grandić D, Šćulac P (2012). Effective Stiffness for Structural Analysis of Buildings in Earthquake. *4th International Conference Civil Engineering-Science and Practice*, Žabljak, 20-24 February, 811-818.

Wong JM, Sommer A, Briggs K, Ergin C (2017). Effective stiffness for modeling reinforced concrete structures: a literature review. *Structure Magazine*, Jan, 2017, 18-21.

Yuksel SB, Foroughi S (2019). Analytical investigation of confined and unconfined concrete strength of RC columns. *Konya Journal of Engineering Sciences*, 7(3), 612-631.

Challenge Journal of Structural Mechanics

Research Article

Evaluation of the period and soft story conditions of reinforced concrete buildings with and without infill walls

Başak Zengin [a]

[a] *Department of Construction Technology, Elbistan Vocational High School, Kahramanmaraş İstiklal University, 46340 Kahramanmaraş, Turkey*

ABSTRACT

Since the ground floor of most of the buildings in our country is designed as a shop or ground floor (in the buildings created as a workplace), there is very little infill wall ratio on the ground floors due to architectural and functional reasons, and some of them do not even exist at all. However, infill walls significantly increase the horizontal rigidity and strength of the structure, thus causing a decrease in the period value that determines the earthquake loads that will affect the structure. However, the infill wall meets the first destructive forces of the earthquake, and during this time, it cracks and absorbs some of the earthquake energy. The structural system elements of the building (columns and shear walls) start to meet the earthquake forces only when the infill walls are damaged and fail. In this direction, the aim of this study is to investigate to what extent the amount of infill wall on the ground floor affects the period of the building, and whether there are soft storey irregularities in the building according to the change in the amount of infill wall on the ground floor. In this study, while there are infill walls on all floors and all axes of buildings of various heights (3, 6, 9 and 11 floors), the amount of infill walls in the x and y directions on the ground floors is reduced to a certain extent, and many models are created until the ground floor is completely without infill walls. All these models created were analyzed with the support of the SAP2000 program, and the period values were determined and examined according to the soft storey problems and compared with the case of the entire building with and without infill walls. In addition, it was examined whether the period formulas determined as a result of the studies and taking into account the infill wall give realistic results for the situation examined in this study.

ARTICLE INFO

Article history:
Received 8 July 2021
Revised 16 August 2021
Accepted 22 August 2021

Keywords:
Reinforced concrete buildings
Infill wall
Period
Soft storey irregularities

1. Introduction

Today, in the design and analysis of buildings, the effects of infill walls, which are defined as non-structural elements, on building behavior are often neglected. However, infill walls have properties that affect dynamic characteristics such as mode shape, damping and vibration period in buildings. In addition, the fact that the contribution of the infill walls to the horizontal rigidity is not taken into account in the calculations gives rise to the thought of staying on the safe side, the distribution and ratio of the infill walls in the floor; It can cause some negativities such as torsional irregularity, short column, soft storey irregularity (Köse and Karslıoğlu 2007; Kose 2009). For this reason, infill walls should be considered during the design and analysis of buildings in order to obtain the true structural behavior.

This increase in stiffness during an earthquake can increase the base shear force demand of the structure and cause greater earthquake forces to act on the structure. Damages in infill walls mean the damping of earthquake energy, which requires infill walls to be taken into account in analytical models. In the literature study, it has been seen that there are many studies that reveal the effect of infill walls on the earthquake behavior of reinforced concrete buildings. The approaches proposed by

* *Corresponding author*. E-mail address: basak.zengin@istiklal.edu.tr (B. Zengin)
ISSN: 2149-8024 / DOI: https://doi.org/10.20528/cjsmec.2021.03.004

TEC-2007 and Hendry were used to model infill walls with equivalent pressure bar. As a result of the study, it was determined that the infill walls changed the rigidity of the structure, thus reducing the period, relative story drift and shear force on the columns, and increasing the base shear force (Sağlıyan, 2018).

In the research of Akyürek et al. (2018), residential type reinforced concrete buildings with different number of spans and floors were chosen as models. The seismic performance of these buildings, which are designed with and without infill walls, was made using the linear inelastic evaluation method. The effects of infill wall amount and placement change on the building's capacity curve, first natural period, target displacement request, damage distribution of the first-floor columns, and building performance level were examined on the selected buildings. The results showed that the infill wall placement significantly affects the building behavior. Therefore, in order to obtain more accurate results in describing the earthquake performance of buildings, infill walls should be taken into account in the analysis. That is also important to emphasize the importance of correctly defining the characteristics of the infill wall (Akyürek et al., 2018).

By Furtado et al. (2017), it is emphasized that most of the damages in reinforced concrete buildings in earthquake zones are caused by infill walls, infill walls significantly affect the earthquake behavior of the building and cause different collapse mechanisms in the building. For this reason, an experimental study was carried out in order to observe in-plane and out-of-plane infill wall damages. In the report published as a result of the Van-Edremit earthquake that took place in 2011, it is stated that in the case of structures with infill walls made of hollow bricks, if the drift ratio between floors exceeds approximately 0.5% - 0.7%, the partition walls are crushed and/or toppled out of its plane, and as a result, the damage observed in the structural system increases. Koçak (2013) investigated the short column damages caused by infill walls in a reinforced concrete building damaged in the 1992 Erzincan earthquake.

By Ning et al. (2017), as a result of the analytical studies they carried out to investigate the effects of infill walls used in buildings on the performance of load-bearing system elements, they determined that infill walls affect the collapse mechanisms of buildings and plastic hinge positions. Qian and Li (2017) investigated the effects of infill wall on the failure mechanisms and load-displacement curves of the frames in their experimental studies on infilled and non-infilled frames. Asteris et al. (2011) and Asteris (2003) presented a reduction parameter to the equivalent pressure bars, which are widely used in the modeling of infill walls in the literature, in order to reflect the voids in the infill walls. For this purpose, they used analytical models that they updated according to the data obtained from various experimental studies. In the study of Güler et al. (2008), effect of infill wall on the building period was studied and they considered a twelve-storey building without infill wall, with infill wall (unplastered) and infill wall (plastered). Using the microtremor (small vibration measurements) method, for all these cases, they found the periods of the structure in small ground motion (not taking into account the earthquake effect) in the two earthquake directions.

In Borekçi's study (2019), the dominant period of a building consisting of 6-storey reinforced concrete frames, which is thought to represent the building stock in Turkey, was obtained both analytically and directly by formulas by modeling in the SAP2000 program. In this study, in which the building periods are obtained with two different models, with and without walls, the approaches of the proposed formulas in obtaining the period and how much they take into account the wall effect were investigated. In buildings with few floors and no irregularities, the dominant mode is the translation mode, and it is possible to consider such buildings as a single degree of freedom. Since a single mode can be used in the design of buildings under seismic loads whose displacement mode can be considered as dominant and equivalent single degree of freedom, it will be sufficient to obtain only the period of this mode. Direct formulas that will help to obtain this period quickly without the need for long calculations have been proposed in various studies in the literature. Walls are built in order to create rooms in buildings and it is clear that these walls will change the period with their contribution to rigidity. However, during the design, the contribution of the walls to the rigidity is neglected and only the weight is taken into account. While some of the direct formulas proposed in the literature to obtain the period do not take into account the effect of the wall, some take into account the contribution of the wall stiffness.

In the modeling studies on infill walls, the properties of the materials or the form of construction caused differences in the period. By Lemonis et al. (2019), the proposed model was evaluated parametrically against the numerical results obtained from the frame analyzes with varying number of frame plies, infill openings, wall thickness and modulus of elasticity. Evaluation of the proposed model was performed against regular frames with uniform infill properties across all of its panels. No deterioration in filling properties was observed. They found that more research is needed for frames with irregularities in their structural form or walls, particularly where a soft ply is created. In Asteris et al.'s study (2015), this article examines the foundation vibration period of reinforced concrete buildings through finite element macro modeling and modal eigenvalue analysis. As a baseline study, a large number of 14-storey reinforced concrete buildings were rated as "designed according to code" and "not designed according to code". Various parameters were examined, including the number of apertures; span length in the direction of movement; hardness of fillings; percentage openings of fillings and; location of soft floors. The calculated values of the fundamental period are compared with the values obtained from the seismic codes and equations proposed by various researchers in the literature. From the analysis of the results, it has been found that the span length, the stiffness of the infill wall panels and the position of the soft floors are very important parameters that affect the foundation period of reinforced concrete buildings. In a different study by Asteris (2015), it was found that the number of

floors, span length, rigidity of infill wall panels, location of soft floors and floor type are very important parameters that affect the foundation period of reinforced concrete buildings. Asteris further developed his research (2016, 2019) and estimated the base periods with neural network support. By Asteris (2017), effect of the number of floors, number of spans, span length, infill wall panel stiffness and percentage of openings in the infill panel on the foundation period of infilled reinforced concrete frames were investigated. Based on these results, a regression analysis is applied to propose a new empirical equation for the estimation of the fundamental period. The derived equation has been shown to be better. Predictive power compared to equations are available in the literature.

The aim of the present work is to investigate the period of vibration of 3, 6, 9 and 11 floors-storey bare and infilled RC frame building by means of finite element modelling under various geometric and other parameters, including the influence of the number of storey, the floor irregularities as well as the soft storey position.

2. Material and Method

In this section, the effects of the changes in the ratio of the infill walls on the ground floor on the period of the building in infilled buildings are examined. As a result of the analyzes made on building models with different heights and different sizes of load-bearing systems, varying period values depending on the rate of change of the infill wall on the ground floor were obtained, these values were interpreted and compared with the results obtained from the period formulas considering the infill wall (Fig. 1).

The axial stiffness of the crossbars was determined by Ersin's (1997) formula for the axial stiffness of infill walls. In this study, while determining the axial stiffness of the crossbars, window openings on the outer walls and door openings on the inner walls were taken into account, and parameters such as the plastered infill wall elasticity modulus, wall thickness, and the length of the cross were used.

$$w = \alpha \cdot L_d \tag{1}$$

where E is the elastic modulus of the wall, t is the thickness of the wall, and w is the width of the wall.

$$EF = E \cdot t \cdot \alpha \cdot L_d \tag{2}$$

where L_d is the diagonal length of the infill wall, and α is the coefficient that allows the pendulum bar width to be defined according to the infill wall diagonal length.

This expression is multiplied by a factor such as β to include void infill walls and γ to take all other effects into account.

$$EF = E \cdot t \cdot \alpha \cdot L_d \cdot \beta \cdot \gamma \tag{3}$$

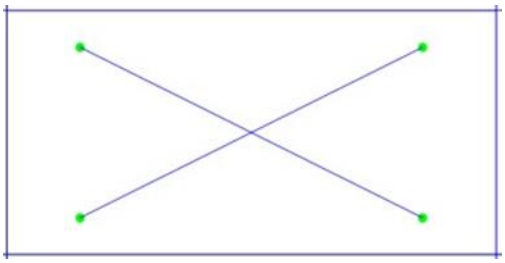

Fig. 1. A pair of articulated crossbars representing the infill wall.

In the four different building models created, the infill walls on the ground floor were reduced at certain rates, and analyzes of the models in each case were examined in detail. As a result of these analyzes, the relationships between this change of the infill wall on the ground floor and the period values, soft storey irregularity were evaluated.

2.1. Features of the created carrier systems

The plan views of the four different (3, 6, 9, 11 storey) mechanical building models are the same, but the building heights are different. The floor thickness is fixed in each building model and on each floor and is 15 cm. Concrete class C25 and reinforced concrete steel class S420 concrete were used in all structures. Floor heights in all buildings are fixed and 3 m. All four building models have 4 openings in the x direction and 5 openings in the y direction (Table 1).

Table 1. Building elements case.

Building	Storey	Square Column	Rectangle Column	Beam
3 Storey	1. 2.	45/45	40/45	35/40
	3.	40/40	40/40	35/40
6 Storey	1. 2.	55/55	40/55	35/55
	3. 4.	50/50	40/50	35/50
	5. 6.	45/45	40/45	35/45
9 Storey	1. 2. 3.	55/55	40/55	35/55
	4. 5. 6.	50/50	40/50	35/50
	7. 8. 9.	45/45	40/45	35/45
11 Storey	1. 2. 3.	60/60	40/60	35/60
	4. 5. 6.	55/55	40/55	35/55
	7. 8. 9.	50/50	40/50	35/50
	10. 11.	45/45	40/45	35/45

The ground periods used in the spectral analysis of all these models were taken as Ta=0.15 and Tb=0.40. In this model, in which infill walls are not included in the mechanical model, equivalent cross-pressure bars represented by infill walls are placed, and the fully infill wall model in Fig. 2 is created.

From the completely infilled model created in each building model, new models were created by reducing the infill wall areas only on the ground floor, and the analyses were repeated.

2.2. No infill wall in the system (bare frame)

In this model, the entire building is designed without infill walls and any element representing the infill wall is not reflected in the mechanical model (Fig. 3).

In this model, the entire building is designed with infill walls, and the elements representing the infill wall with spaces (door, window) on each axis in the x and y directions are reflected in the mechanical model (Figs. 4 and 5).

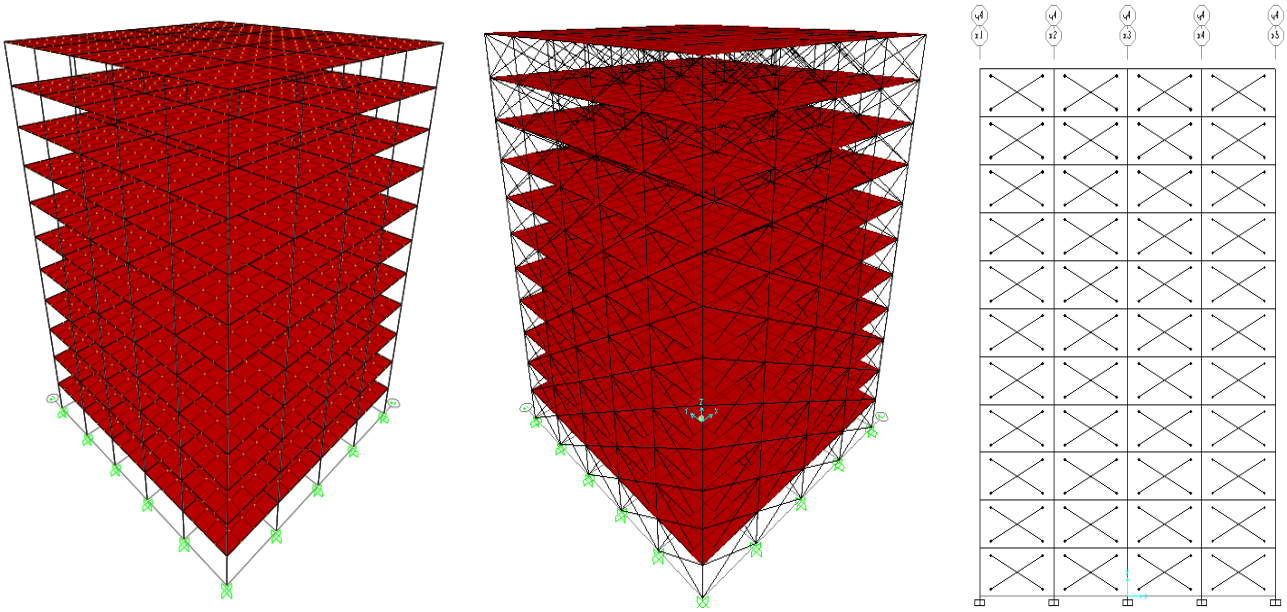

Three-dimensional view of the 11-storey building without walls created in SAP2000

Section view of the fully infilled wall model created in SAP2000 of the 11-storey building

Cross Section

Fig. 2. Storey building of modelling image.

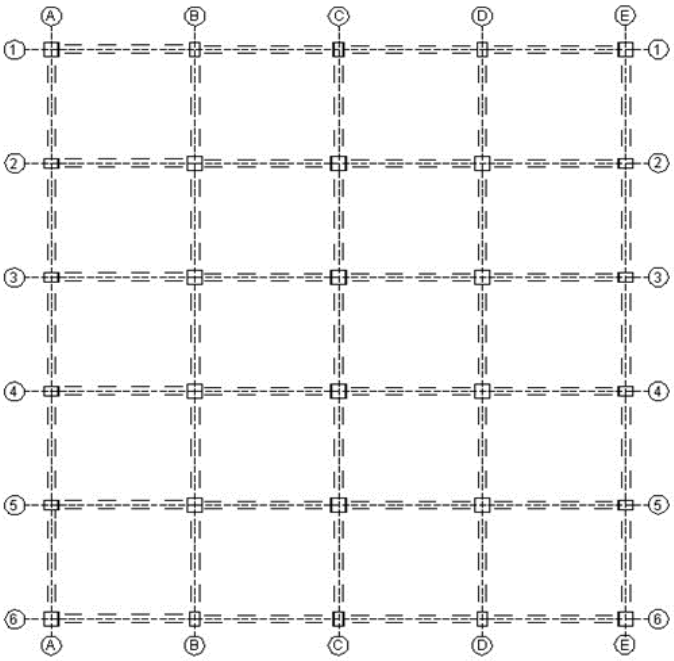

Fig. 3. No walls in the building plan.

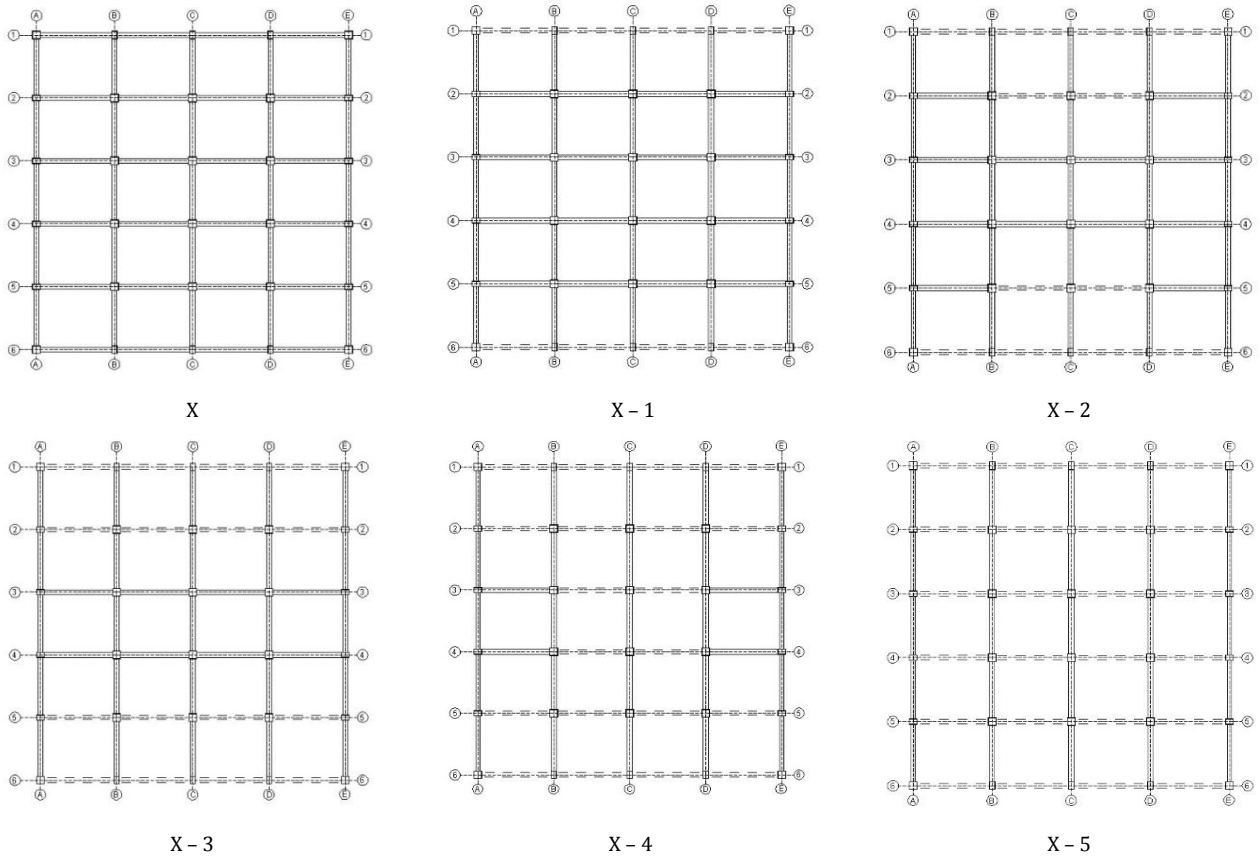

Fig. 4. The case of infill walls in all of the building frames (plan image *x*-*x*).

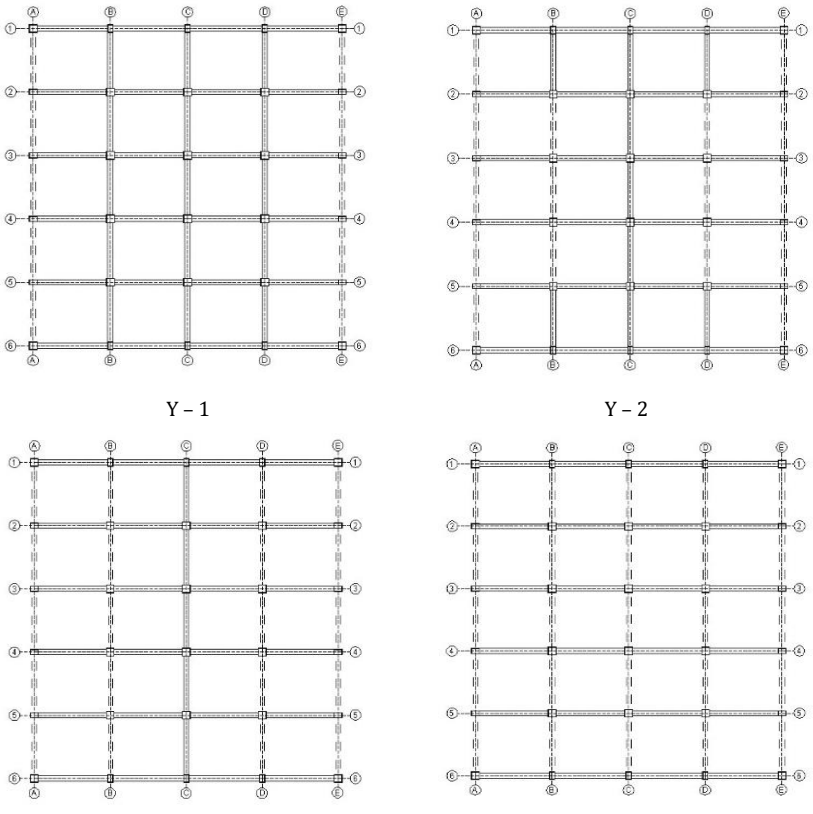

Fig. 5. The case of infill walls in all of the building frames (plan image *y*-*y*).

In this model, the absence of infill walls in all of the A and E axes in the *y-y* direction only on the ground floor is reflected in the model. Except for the ground floor, the plan views of all floors are the same as the plan view of the fully infilled model. The ground floor plan view is as in Fig. 5.

3. Investigation of the Period Values of the Models Created

3.1. Examining the analysis results

Analysis results for 3, 6, 9 and 11 storey buildings show that; the period of the entire structure with infill walls is much smaller than the period when the structure is completely without infill walls (bare frame). In addition, it is seen that the decrease in the infill wall ratios in the x and y directions only on the ground floor increases the periods of the building in the *x* and *y* directions (although not as much as the periods in the bare frame situation). As a result of this period change, it is seen that the period decreases rates compared to the bare frame decrease due to this decrease as the amount of infill wall decreases on the ground floor. Below is the graph showing the period decrease rates in all cases, which express the change in the amount of infill walls on the ground floors of the 3, 6, 9 and 11 storey buildings, depending on A_k (infill wall/ (infill wall + load-bearing system)).

As can be seen from the Fig. 6 graph, the change in the amount of infill wall on the ground floor mostly affects the period of 3-storey buildings, while this effect is very low in 11-storey structures. In other words, as the number of floors increases, the effect of the infill wall reductions on the ground floor to increase the period of the building decreases.

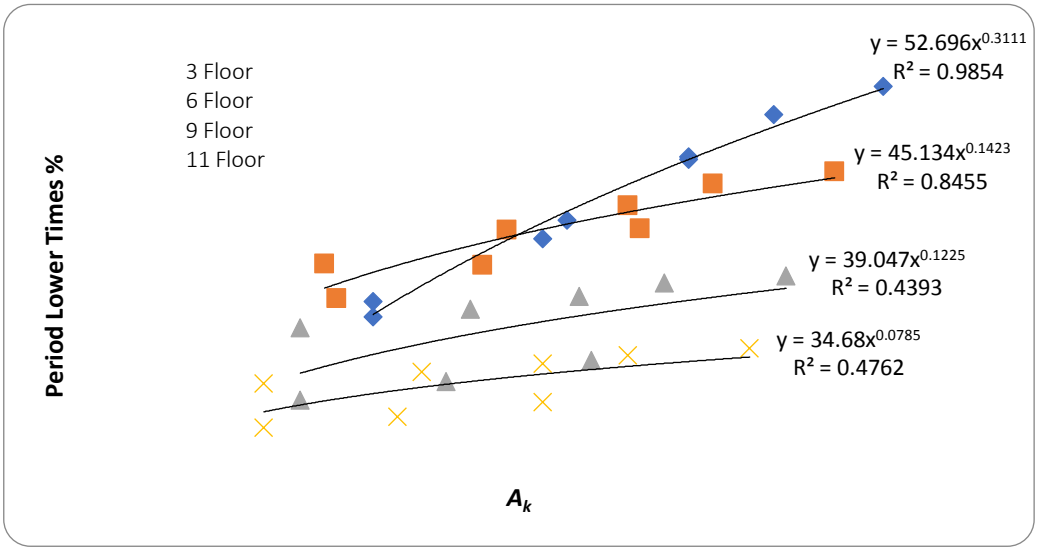

Fig. 6. Relationship between reduction of infill wall area and period reduction in all buildings.

The comparison of the period values obtained from this study with the formulas obtained in other studies is given in Table 2. While the period values obtained as a result of the formula obtained by the infill walls depending on the change in all floors give the same result for the bare frame and all-walled cases, they give higher results than the period values obtained depending on the reduction amount of the infill wall on the ground floor. This result is quite natural since the change of the infill wall only on the ground floor cannot be compared with the change in the amount of infill wall on all floors. The period values obtained as a result of the infill wall reduction on the ground floor are slightly larger than the period values in the completely walled condition, except for the 3-storey building. The results obtained from the other period formulas that take into account the infill wall, on the other hand, are closer to (slightly lower than these periods) the periods of the buildings in the bare frame condition. From these results, it is understood that using the period formulas that take into account the proposed infill wall will not give realistic results for cases where the infill wall is reduced only on the ground floor.

Investigation of soft storey irregularity formation conditions of the created models provides analysis results for 3-storey building in Table 3.

Cases of soft floor irregularities of buildings;

If $\eta c_i = (\Sigma A_e)_i \,/\, (\Sigma A_e)_{i+1} < 0.80$, there is soft storey irregularity.

Definition of effective cutting area on any floor:

$$\sum A_e = \sum A_w + \sum A_g + 0.15 \sum A_k \qquad (4)$$

where ηc_i is the strength irregularity coefficient defined at *i*th floor, ΣA_e is the effective shear area at any floor in the direction of the earthquake under consideration, A_w is the effective area of the column cross-section (excluding the area of the column projections perpendicular to the earthquake), ΣA_w is the sum of effective body areas A_{ws} of column cross-section at any storey, ΣA_g is the sum of the cross-sectional areas of the structural system elements operating as a shear parallel to the earthquake direction considered at any floor, and ΣA_k is the sum of the masonry infill wall areas (excluding door and window spaces) parallel to the earthquake direction considered at any floor.

Table 2. Period comparison.

		Study		Koçak et al. (2011, 2018)		Guler et al. (2008)	TEC-1998	UBC-1997	Goel and Chopra (1997)	
		Tx	*Ty*	*Tx*	*Ty*				Lower Limit	Top Limit
3 Storey	Frame	0.476	0.447	0.476	0.447					
	Frame+Wall	0.251	0.244	0.247	0.245					
3 Storey XX direction	X-1	0.258	0.244	0.279	0.245					
	X-2	0.269	0.244	0.304	0.245					
	X-3	0.284	0.244	0.338	0.245					
	X-4	0.304	0.244	0.392	0.245	0.329	0.364	0.38	0.34	0.484
	X-5	0.333	0.244	0.476	0.245					
3 Storey YY direction	Y1	0.251	0.252	0.247	0.285					
	Y2	0.251	0.271	0.247	0.324					
	Y3	0.251	0.289	0.247	0.368					
	Y4	0.251	0.324	0.247	0.447					
6 Storey	Frame	0.798	0.744	0.798	0.744					
	Frame+Wall	0.456	0.440	0.438	0.430					
6 Storey XX direction	X-1	0.461	0.440	0.497	0.430					
	X-2	0.470	0.440	0.538	0.430					
	X-3	0.480	0.440	0.596	0.430					
	X-4	0.494	0.440	0.680	0.430	0.619	0.612	0.639	0.634	0.903
	X-5	0.513	0.440	0.798	0.430					
6 Storey YY direction	Y1	0.456	0.447	0.438	0.496					
	Y2	0.456	0.461	0.438	0.566					
	Y3	0.456	0.474	0.438	0.628					
	Y4	0.456	0.496	0.438	0.744					
9 Storey	Frame	1.038	0.934	1.038	0.934					
	Frame+Wall	0.649	0.619	0.600	0.561					
9 Storey XX direction	X-1	0.653	0.619	0.677	0.561					
	X-2	0.660	0.619	0.730	0.561					
	X-3	0.667	0.619	0.797	0.561					
	X-4	0.677	0.619	0.898	0.561	0.884	0.829	0.866	0.913	1.301
	X-5	0.689	0.619	1.038	0.561					
9 Storey YY direction	Y1	0.649	0.625	0.600	0.650					
	Y2	0.649	0.635	0.600	0.731					
	Y3	0.649	0.644	0.600	0.808					
	Y4	0.649	0.659	0.600	0.934					
11 Storey	Frame	1.151	1.070	1.151	1.070					
	Frame+Wall	0.763	0.735	0.691	0.674					
11 Storey XX direction	X-1	0.767	0.735	0.776	0.674					
	X-2	0.767	0.735	0.835	0.674					
	X-3	0.772	0.735	0.917	0.674					
	X-4	0.777	0.735	1.019	0.674	1.058	0.964	1.006	1.093	1.559
	X-5	0.792	0.735	1.151	0.674					
11 Storey YY direction	Y1	0.764	0.739	0.691	0.776					
	Y2	0.764	0.747	0.691	0.867					
	Y3	0.764	0.753	0.691	0.947					
	Y4	0.764	0.762	0.691	1.070					

In Table 3, the strength irregularity coefficients of the ground floor of all models created for the 3-storey building are given. When the results are examined, it is seen that these coefficients decrease in the x and y directions due to the reduction of the infill wall in the x and y directions. It is seen that the strength irregularity coefficients take the values of 0.785, 0.742, 0.771, (0.742 and 0.771) respectively in the X-4, X-5, Y-4th and ground floor unwalled cases, and it is understood that soft storey irregularity occurs in these models.

In Table 4, the strength irregularity coefficients of the ground floor for all models created for the 6-storey building are given. When the results are examined, it is seen that these coefficients decrease in the x and y directions due to the reduction of the infill wall in the x and y directions. It is seen that the strength irregularity coefficients take the value of 0.774 in both the X-5th and ground floor unwalled cases, and it is understood that weak floor irregularity occurs in these models.

Table 3. Analysis results of 3-storey building models.

Cases		ΣA_w (m²)	ΣA_k (m²) (X Direction)	ΣA_k (m²) (Y Direction)	ΣA_e (m²) (X Direction)	ΣA_e (m²) (Y Direction)	η_{c1} (X Direction)	η_{c1} (Y Direction)	Soft Storey Irregularity
Ground Storey	Frame+Wall	5.76	13.35	11.42	77.625	7.473	1.000	1.000	No
	X-1	5.76	8.88	11.42	7.092	7.473	0.914	1.000	No
	X-2	5.76	6.66	11.42	6.759	7.473	0.871	1.000	No
	X-3	5.76	4.44	11.42	6.426	7.473	0.828	1.000	No
	X-4	5.76	2.22	11.42	6.093	7.473	0.785	1.000	Available
	X-5	5.76	0	11.42	5.760	7.473	0.742	1.000	Var
	Y-1	5.76	13.35	6.83	77.625	67.845	1.000	0.908	No
	Y-2.	5.76	13.35	4.10	77.625	6.375	1.000	0.853	No
	Y-3	5.76	13.35	2.28	77.625	6.102	1.000	0.817	No
	Y-4	5.76	13.35	0	77.625	5.760	1.000	0.771	Available
	Non Wall	5.76	0	0	5.760	5.760	0.742	0.771	Available
	Frame	5.76	0	0	5.760	5.760	1.000	1.000	No
First Strorey	Frame+Wall	5.76	13.35	11.42	77.625	7.473	-	-	-
	Frame	5.76	0	0	5.760	5.760	-	-	-

Table 4. Analysis results of 6-storey building models.

Cases		ΣA_w (m²)	ΣA_k (m²) (X Direction)	ΣA_k (m²) (Y Direction)	ΣA_e (m²) (X Direction)	ΣA_e (m²) (Y Direction)	η_{c1} (X Direction)	η_{c1} (Y Direction)	Soft Storey Irregularity
Ground Storey	Frame+Wall	6.8	13.26	11.33	8.789	84.995	1.000	1.000	No
	X-1	6.8	8.8	11.33	8.120	84.995	0.924	1.000	No
	X-2	6.8	6.6	11.33	7.790	84.995	0.886	1.000	No
	X-3	6.8	4.4	11.33	7.460	84.995	0.849	1.000	No
	X-4	6.8	2.2	11.33	7.130	84.995	0.811	1.000	No
	X-5	6.8	0	11.33	6.800	84.995	0.774	1.000	Available
	Y-1	6.8	13.26	6.75	8.789	78.125	1.000	0.919	No
	Y-2.	6.8	13.26	4.05	8.789	74.075	1.000	0.872	No
	Y-3	6.8	13.26	2.25	8.789	71.375	1.000	0.840	No
	Y-4	6.8	13.26	0	8.789	6.800	1.000	0.800	No
	Non Wall	6.8	0	0	6.800	6.800	0.774	0.800	Available
	Frame	6.8	0	0	6.800	6.800	1.000	1.000	No
First Strorey	Frame+Wall	6.8	13.26	11.33	8.789	84.995	-	-	-
	Frame	6.8	0	0	6.800	6.800	-	-	-

In Table 5, the strength irregularity coefficients of the ground floor for all models created for the 9-storey building are given. When the results are examined, it is seen that these coefficients decrease in the x and y directions due to the reduction of the infill wall in the x and y directions. It is seen that none of the strength irregularity coefficients are less than 0.8, and it is understood that weak story irregularity does not occur in any of these cases.

In Table 6, the strength irregularity coefficients of the ground floor for all models created for the 11-storey building are given. When the results are examined, it is seen that these coefficients decrease in the x and y directions due to the reduction of the infill wall in the x and y directions. It is seen that none of the strength irregularity coefficients are less than 0.8, and it is understood that weak story irregularity does not occur in any of these cases.

Table 5. Analysis results of 9-storey building models.

Cases		ΣA_w (m²)	ΣA_k (m²) (X Direction)	ΣA_k (m²) (Y Direction)	ΣA_e (m²) (X Direction)	ΣA_e (m²) (Y Direction)	η_{c1} (X Direction)	η_{c1} (Y Direction)	Soft Storey Irregularity
Ground Storey	Frame+Wall	7.92	13.17	11.25	98.955	96.075	1.000	1.000	No
	X-1	7.92	8.72	11.25	9.228	96.075	0.933	1.000	No
	X-2	7.92	6.54	11.25	8.901	96.075	0.899	1.000	No
	X-3	7.92	4.36	11.25	8.574	96.075	0.866	1.000	No
	X-4	7.92	2.18	11.25	8.247	96.075	0.833	1.000	No
	X-5	7.92	0	11.25	7.920	96.075	0.800	1.000	No
	Y-1	7.92	13.17	6.68	98.955	8.922	1.000	0.929	No
	Y-2.	7.92	13.17	4.01	98.955	85.215	1.000	0.887	No
	Y-3	7.92	13.17	2.23	98.955	82.545	1.000	0.859	No
	Y-4.	7.92	13.17	0	98.955	7.920	1.000	0.824	No
	Non Wall	7.92	0	0	7.920	7.920	0.800	0.824	No
	Frame	7.92	0	0	7.920	7.920	1.000	1.000	No
First Strorey	Frame+Wall	7.92	13.17	11.25	98.955	96.075	-	-	-
	Frame	7.92	0	0	7.920	7.920	-	-	-

Table 6. Analysis results of 11-storey building models.

Cases		ΣA_w (m²)	ΣA_k (m²) (X Direction)	ΣA_k (m²) (Y Direction)	ΣA_e (m²) (X Direction)	ΣA_e (m²) (Y Direction)	η_{c1} (X Direction)	η_{c1} (Y Direction)	Soft Storey Irregularity
Ground Storey	Frame+Wall	9.12	13.08	11.16	11.082	10.794	1.000	1.000	No
	X-1	9.12	8.64	11.16	10.416	10.794	0.940	1.000	No
	X-2	9.12	6.48	11.16	10.092	10.794	0.911	1.000	No
	X-3	9.12	4.32	11.16	9.768	10.794	0.881	1.000	No
	X-4	9.12	2.16	11.16	9.444	10.794	0.852	1.000	No
	X-5	9.12	0	11.16	9.120	10.794	0.823	1.000	No
	Y-1	9.12	13.08	6.60	11.082	10.110	1.000	0.937	No
	Y-2.	9.12	13.08	3.96	11.082	9.714	1.000	0.900	No
	Y-3	9.12	13.08	2.20	11.082	9.450	1.000	0.875	No
	Y-4.	9.12	13.08	0	11.082	9.120	1.000	0.845	No
	Non Wall	9.12	0	0	9.120	9.120	0.823	0.845	No
	Frame	9.12	0	0	9.120	9.120	1.000	1.000	No
First Strorey	Frame+Wall	9.12	13.08	11.16	11.082	10.794	-	-	-
	Frame	9.12	0	0	9.120	9.120	-	-	-

4. Conclusions

In this study, it has been investigated to what extent the amount of infill wall on the ground floor affects the period of the building, and whether soft floor and weak floor irregularities occur in the building according to the change in the amount of infill wall on the ground floor. For this research, analyses were made for various situations of 4 types of buildings with 3, 6, 9 and 11 floors. The results obtained are as follows.

- In order to take the infill walls into account in the analyses, it has been seen that representing the infill walls in the load-bearing system of the buildings as a cross-pendulum rod with two ends gives very realistic results.
- In the examined structures, it was observed that the infill walls significantly increased the rigidity of the structure and as a result, they caused a significant decrease in the construction period.
  The 3-storey building was the most affected by the period-reducing effect of the infill wall. The period value obtained when all floors and all axes of the 3-storey building are in infilled condition (all-walled condition) is 47.27% less than the period value obtained when all floors and all axes of the 3-storey structure are without infill walls (bare frame condition).
  The 11-storey building was least affected by the period-reducing effect of the infill wall. The period value obtained when all floors and all axes of the 11-storey building are in infilled state (all-walled state) is 33.71% less than the period value obtained when all floors and all axes of the 11-storey building are without infill walls (bare frame state).
  Even though the period-reducing effect of the infill wall decreases as the structure rises, it is still very large. Regardless of the height of the structure, it should be noted that the infill wall greatly reduces the period of the structure.
- The decrease in the amount of infill wall on the ground floor of a building with infill walls on all floors and all axes (all-walled condition) increases the period of the building somewhat compared to the period of the building with all walls.
  While this increase was significant in the 3-storey building, it was observed that it was too small to be ignored in the 11-storey building. From this, we can conclude that the change in the amount of infill wall only on the ground floor has a large effect on the period of the building in buildings with low height, and negligible effect on the period of the building in buildings with high height. In addition, we can say that this effect increases and decreases inversely with the height of the building (the lower the structure, the greater the effect, the larger the structure, the less the effect).
- It has been seen that the period values obtained from the period formulas that take into account the infill wall effect, which have been revealed as a result of the studies carried out by various people before, do not give appropriate results for all-walled structures where the amount of infill wall changes only on the ground floor.
  In all buildings except the 3-storey building, the periods obtained by reducing the wall on the ground floor are closer to the period of the whole building with walls. Although the values obtained from the other period formulas are between the periods of all the buildings with walls and bare frames, they are quite far from the period values obtained by reducing the wall on the ground floor, except for the 3-storey building.
- Reducing the amount of infill walls only on the ground floors of the buildings considerably increases the relative floor offsets on the ground floors of the buildings.
- In low-rise buildings and in the case of medium-height (6-7-storey) buildings, only the ground floors have very little or no infill walls (all of the other floors are infilled), weak floor irregularities may occur in the ground floor of the buildings. In very high buildings, although the building is completely filled with infill walls, even if there is no infill wall on the ground floor, weak floor irregularities do not occur on the ground floor of the building.

If we want to design earthquake-resistant structures, we need to know the behaviour of structures under the influence of earthquakes and design our structures in the most appropriate way to this behaviour. As can be understood from the results above, the infill walls created to fulfil the architectural and functional functions in a building have a great effect on the behaviour of the building under the influence of earthquakes. Since this effect cannot be neglected in many respects, the infill wall must be reflected in the analysis and calculations in the building design. Otherwise, the reliability of the building may be shaken in many respects, unexpected negativities and even catastrophic destructions may occur under the influence of earthquakes. In this case, ignoring the effects of the infill wall on the structure under the influence of an earthquake can be equivalent to neglecting human life.

From the results of the analysed four different (3, 6, 9, 11 storey) regularity, it was shown that current code equations are unable to accurately predict the effect of horizontal and vertical regularities on the period. It was also shown that structures with vertical irregularities, like a setback, tend to have shorter period than the regular structures and compared formulations. Especially we will try to achieve it by means of regressive techniques, using as data all the above studied parameters and corresponding results, irregularity systems.

References

Akyürek O, Tekeli H, Demir F (2018). Effect of infill wall placement in plan on building performance. *International Journal of Engineering Research and Development*, 10(1), 42-55.

Asteris PG (2003). Lateral stiffness of brick masonry infilled frames. *Journal of Structural Engineering*, 129(8), 1071-1079.

Asteris PG, Chrysostomou CZ, Giannopoulos IP, Smyrou E (2011). Masonry infilled reinforced concrete frames with opening. *III ECCOMAS Thematic Conference on Computational Methods in Structural Dynamics and Earthquake Engineering*, Greece.

Asteris PG, Nikoo M (2019). Artificial bee colony-based neural network for the prediction of the fundamental period of infilled frame structures. *Neural Computing and Applications*, 31(9), 4837-4847.

Asteris PG, Repapis CC, Tsaris AK, Di Trapani F, Cavaleri L (2015). Parameters affecting the fundamental period of infilled RC frame structures. *Earthquake and Structures*, 9(5), 999-1028.

Asteris PG, Repapis C, Cavaleri L, Sarhosis V, Athanasopoulou A (2015). On the fundamental period of infilled RC frame buildings. *Structural Engineering and Mechanics*, 54(6), 1175-1200.

Asteris PG, Tsaris AK, Cavaleri L, Repapis C, Papalou A, Di Trapani F, Karypidis DF (2016). Prediction of the fundamental period of infilled RC frame structures using artificial neural networks. *Computational Intelligence and Neuroscience*, 5104907, 12.

Asteris PG, Repapis CC, Foskolos F, Fotos A, Tsaris AK (2017). Fundamental period of infilled RC frame structures with vertical irregularity. *Structural Engineering and Mechanics,* 61(5), 663-674.

Börekçi M (2019). Obtaining the dominant period of reinforced concrete buildings with infill walls directly by formulas. *Haliç University Journal of Science and Technology,* 2(2), 161-178.

Ersin UD, Yuksel E, Kocak A, Hayashi M, Karadogan F (1998). System identification by means of micro tremor measurements. *Second Japan-Turkey Workshop on Earthquake Engineering*, I–633-648, İstanbul.

Furtado A, Rodrigues H, Arêde A (2015). Modelling of masonry infill walls participation in the seismic behaviour of RC buildings using OpenSees. *International Journal of Advanced Structural Engineering,* 7, 117-127.

Goel RK, Chopra AK (1997). Period formulas for moment resisting frame buildings. *Journal of Structural Engineering*, *ASCE*, 123(11), 1454-1461.

Guler H, Yuksel E, Kocak A (2008). Estimation of the fundamental vibration period of existing RC buildings in Turkey utilizing ambient vibration records. *Journal of Earthquake Engineering,* 12, 140-150.

Koçak A (2013). The effect of short columns on the performance of existing buildings. *Structural Engineering and Mechanics*, 46(4), 505-518.

Koçak A, Börekçi M, Zengin B (2018). Period formula for RC frame buildings considering infill wall thickness and elasticity modulus. *Scientia Iranica Transaction A*, 25(1), 118-128.

Koçak A, Yildirim MY (2011). Effects of infill wall ratio on the period of reinforced concrete framed buildings. *Advances in Structural Engineering*, 14, 731-743.

Kose MM (2009). Parameters affecting the fundamental period of RC buildings with infill wall. *Engineering Structures*, 31(1), 93-102.

Kose MM, Karslıoğlu O (2007). Effects of infill walls on building natural modal period and mode shape. *6th National Conference on Earthquake Engineering*, İstanbul.

Lemonis ME, Asteris PG, Zitouniatis DG, Ntasis GD (2019). Modelling of the lateral stiffness of masonry infilled steel moment-resisting frames. *Structural Engineering and Mechanics,* 70(4), 421-429.

Ning N, Yu D, Zhang C, Jiang S (2017). Pushover analysis on infill effects on the failure pattern of reinforced concrete frames. *Applied Sciences,* 7(4), 428.

Qian K, Li B (2017). Effects of masonry infill wall on the performance of RC frames to resist progressive collapse. *Journal of Structural Engineering*, 143(9), 04017118.

Sağlıyan S (2018). The Effect of modelling approaches of infill walls on reinforced concrete frame behaviour. *Science and Engineerig Journal of Fırat University*, 30(2), 165-174.

SAP2000 (2021). Structural Analysis Program. Computer and Structures, USA.

TBDY-2018 (2018). Turkish Building Earthquake Regulation. Ministry of Environment and Urbanization, Ankara, Turkey.

TEC-1998 (1998). Turkish Earthquake Regulation, Ministry of Public Works and Settlement, Ankara.

UBC-1997 (1997). Uniform Building Code, Structural Design Requirements. International Code Council, International Conference of Building Officials.